



Brainstem neurons that command mammalian locomotor asymmetries

Jared M. Clegg^{ID}¹, Roberto Leiras^{ID}¹, Alexia Montalant¹, Paulina Wanken¹, Ian R. Wickersham^{ID}² and Ole Kiehn^{ID}^{1,3}✉

Descending command neurons instruct spinal networks to execute basic locomotor functions, such as gait and speed. The command functions for gait and speed are symmetric, implying that a separate unknown system directs asymmetric movements, including the ability to move left or right. In the present study, we report that *Chx10*-lineage reticulospinal neurons act to control the direction of locomotor movements in mammals. *Chx10* neurons exhibit mainly ipsilateral projection, and their selective unilateral activation causes ipsilateral turning movements in freely moving mice. Unilateral inhibition of *Chx10* neurons causes contralateral turning movements. Paired left-right motor recordings identified distinct mechanisms for directional movements mediated via limb and axial spinal circuits. Finally, we identify sensorimotor brain regions that project on to *Chx10* reticulospinal neurons, and demonstrate that their unilateral activation can impart left-right directional commands. Together these data identify the descending motor system that commands left-right locomotor asymmetries in mammals.

Locomotion is a natural behavior universal to the animal kingdom. In vertebrates, coordination of rhythmic locomotor movements occurs largely within circuits of the spinal cord itself^{1–4}. For these circuits to function, they need commands from supraspinal effector neurons that control the start and speed of locomotion. The brainstem command neurons that control these parameters have been examined extensively in several vertebrate species^{5–14}. Recently, brainstem neurons that mediate locomotor stop have also been identified^{7,12,13}.

Characteristically, when start command pathways of the midbrain locomotor region are activated unilaterally, they cause bilateral, full-bodied locomotion, which proceeds in a straight line^{7–11,15,16}. This finding underscores symmetry in the command for initiating locomotion and controlling its speed. The anatomic basis for this symmetry has been worked out in some detail. At the level of the midbrain locomotor region, which comprises glutamatergic neurons in the cuneiform and pedunculopontine nuclei, neurons exhibit extensive commissural connectivity with neurons of the contralateral side^{6,8}. The start command is then relayed bilaterally to reticulospinal neurons^{7,8,15}, including those of the lateral paragigantocellular nucleus (LPGi), which in turn activate spinal locomotor circuits^{7,15,17–20}. Neurons of the LPGi project bilaterally, innervating both sides of the spinal cord, and unilateral optogenetic activation of LPGi glutamatergic neurons initiates symmetric, full-bodied locomotion⁷.

A considerable gap in our knowledge is the inability to explain how command neurons direct locomotor movements to the left or right side²¹. A system that executes left-right locomotor asymmetries would be required for any goal-directed locomotor movement, as might occur during basic behaviors such as foraging, navigation and/or escape, but also during specialized locomotor tasks²². From in vitro studies, it is clear that rhythmogenic modules can operate independently within the left or right spinal cord in mammals^{23–27}. Nevertheless, differential engagement of left-right rhythmogenic modules cannot be mediated by a symmetric start command.

Moreover, a unilateral lesion of the corticospinal tract (that is, unilateral pyramidalotomy) does not result in any overt left-right locomotor or postural asymmetries^{28,29}. Although unilateral labyrinth ablation or vestibulocochlear nerve (VIII) stimulation can initiate reflexive rotational behavior³⁰, this self-righting reflex is not considered to be a voluntary locomotor command.

In the present study, we hypothesized that a turn in mammals could be implemented by a system of nucleus gigantocellularis (Gi) reticulospinal neurons defined by expression of *Chx10* (*Vsx2*)¹². These *Chx10* Gi neurons are glutamatergic, and their bilateral activation arrests locomotion by suppressing locomotor rhythrogenesis in the spinal cord¹²; however, it is unknown whether *Chx10* Gi neurons exhibit symmetric or asymmetric engagement of downstream spinal networks. We found that *Chx10* Gi neurons: (1) exhibit dominant unilateral projection to the spinal cord, (2) define the direction of locomotion by effecting changes in ipsilateral limb and axial movements *in vivo*, and (3) can be engaged to impart asymmetric movements via unilateral input from distinct sensorimotor brain regions. *Chx10* Gi neurons exhibit all the features of a bona fide system for executing left-right locomotor asymmetries in mammals.

Results

***Chx10* Gi neurons form a prominent spinal tract of ipsilaterally projecting axons.** For *Chx10* Gi neurons to regulate locomotor movements unilaterally, they should exhibit predominant unilateral projection to the spinal cord. We examined this by labeling *Chx10*-lineage neurons of the rostral Gi with an anterograde viral tracer (*Chx10*^{Cre} > AAV-FLEX-tdTomato-2A-synGFP) (Fig. 1a). In adult mice, a unilateral injection labeled *Chx10* Gi neurons mainly on the same side (93.6 ± 3.1%, Fig. 1b–d). *Chx10* neurons projected axons caudally (Extended Data Fig. 1a,b), which then coalesced to form a prominent ipsilateral tract of axons lateral to the inferior olive (Extended Data Fig. 1c). At the level of the pyramidal decussation, this tract of *Chx10* reticulospinal axons turned ventrally to

¹Department of Neuroscience, Faculty of Health and Medical Sciences, University of Copenhagen, Copenhagen, Denmark. ²The McGovern Institute for Brain Research, Massachusetts Institute of Technology, Cambridge, MA, USA. ³Department of Neuroscience, Karolinska Institutet, Stockholm, Sweden.
✉e-mail: Ole.Kiehn@sund.ku.dk

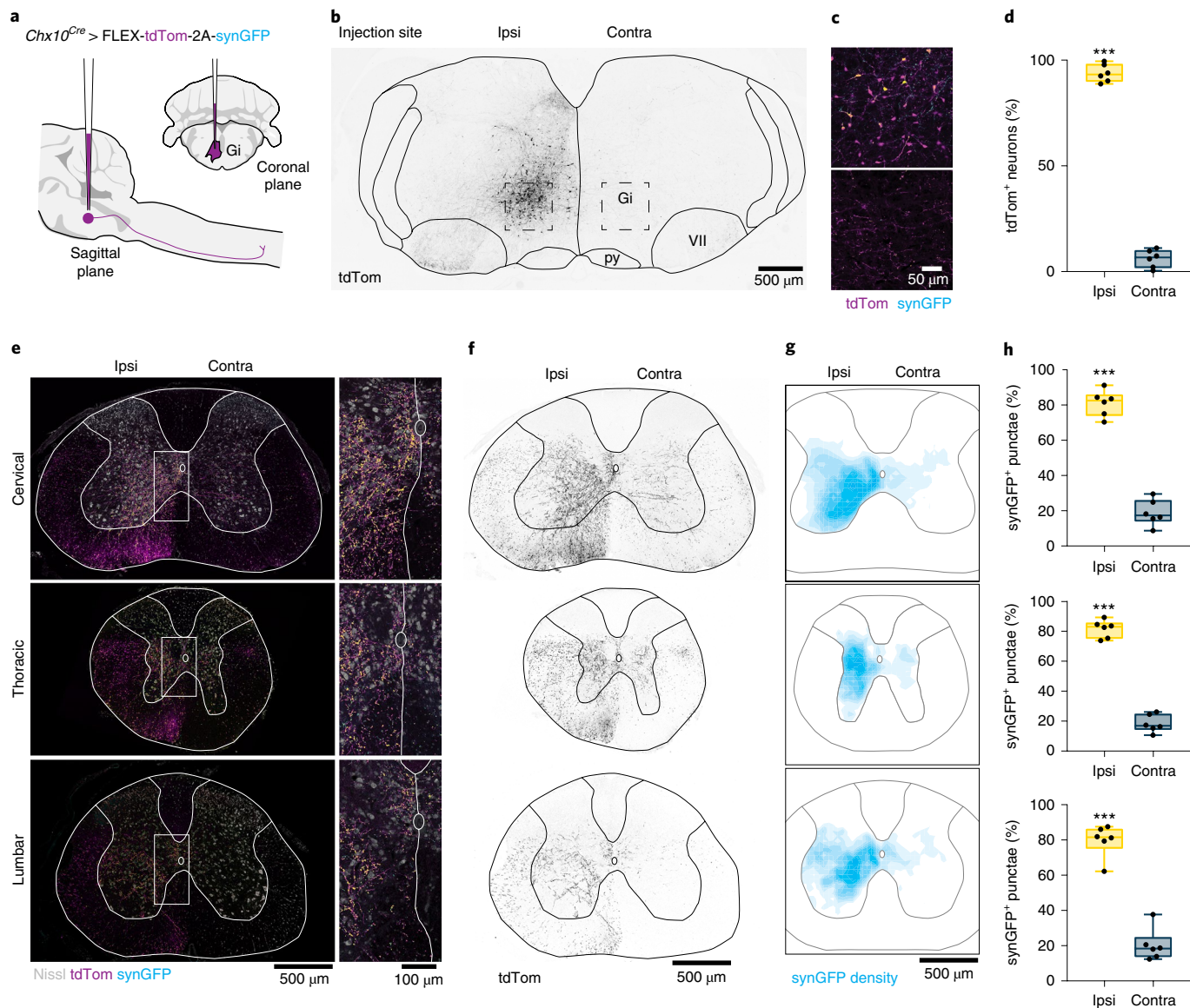


Fig. 1 | Chx10 Gi neurons form a prominent tract of descending axons that project ipsilaterally. **a**, Unilateral labeling of *Chx10* neurons of the rostral Gi using the Cre-dependent anterograde tracer AAV-FLEX-tdTom-2A-synGFP. **b**, Inverted fluorescent image of tdTomato⁺ (tdTom⁺) neurons at the injection site within Gi. **c**, Top: tdTom⁺synGFP⁺ neurons at injection site. Bottom: sparse tdTom⁺ axonal labeling and synGFP⁺ punctae contralateral to the injection site. **d**, Quantification of tdTom⁺ neurons labeled ipsilateral (Ipsi) and contralateral (Contra) to the injection site (**P<0.001; paired, two-tailed Student's t-test; n=6 mice from two independent experiments). **e**, Left: a prominent tract of tdTom⁺ axons is observed within the ventrolateral funiculus of the cervical (top), thoracic (middle) and lumbar (bottom) spinal cord. Axons project almost exclusively on the ipsilateral side. SynGFP⁺ punctae (overlap of cyan with magenta yields yellow) exhibit a high density on the ipsilateral side. Right: insets from images on the left demonstrate a sharp division in the density of axon profiles and synGFP⁺ punctae between the ipsilateral and contralateral sides. **f**, Inverted fluorescent images of tdTom⁺ axonal projections in the cervical (top), thoracic (middle) and lumbar (bottom) spinal cord. Axons descend in the ventrolateral funiculus within a well-defined wedge. **g**, Density plots for synGFP⁺ punctae within the gray matter of the cervical (top), thoracic (middle) and lumbar (bottom) spinal cord (average from six mice). The density of putative synapses is greatest in the intermediate gray matter—laminae VII, VIII and X. SynGFP⁺ punctae were found predominantly on the ipsilateral side and were excluded from laminae I–VI of the dorsal horn, lamina IX (motor neurons) and, at the thoracic level, Clarke's column. **h**, Quantification of synGFP⁺ punctae within the ipsilateral and contralateral spinal cord gray matter (cervical, ***P=0.001; thoracic, ***P<0.001; lumbar, ***P<0.001; paired, two-tailed Student's t-test; n=6 mice from two independent experiments). Data are plotted with box-and-whisker plots, which give the median, 25th and 75th percentiles, and range.

occupy the ipsilateral ventral funiculus within the rostral-most segment of the spinal cord (Extended Data Fig. 1c). TdTomato⁺ axons arborized predominantly within the ipsilateral cord (Fig. 1e,f), with some arborizations on the contralateral side.

We quantified the position and density of *Chx10* Gi synGFP⁺ punctae (putative synapses) within the spinal cord. A majority of

synGFP⁺ punctae were ipsilateral to the injection site (Fig. 1g,h and Supplementary Table 1). The density of synGFP⁺ punctae was greatest in the ipsilateral intermediate gray (laminae VII, VIII and X) (Fig. 1g,h), with the exception of Clarke's column (Th1 to L3) (Fig. 1g,h), a medial nucleus that conveys proprioceptive inputs to the cerebellum. Notably, synGFP⁺ punctae were largely absent

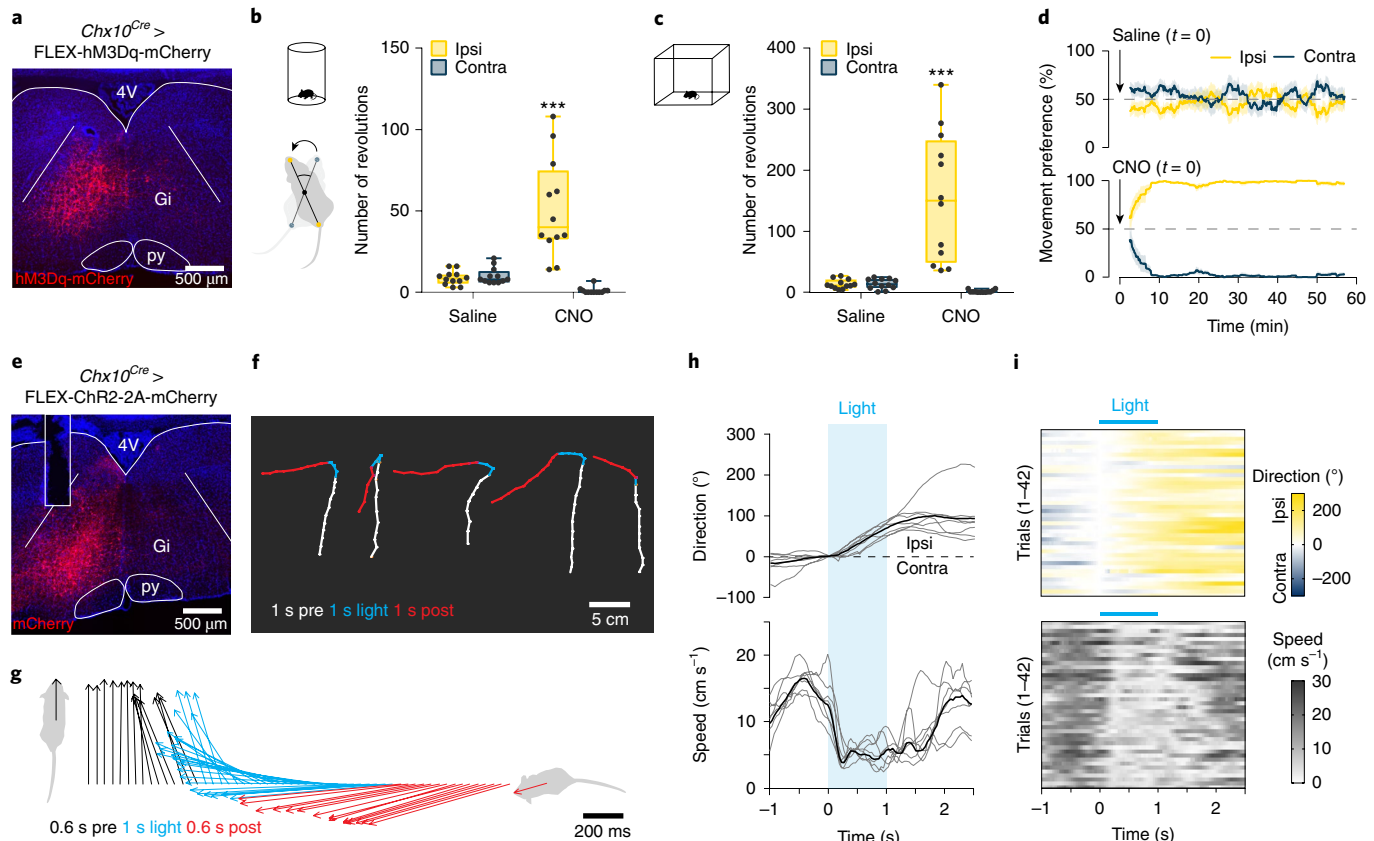


Fig. 2 | Unilateral excitation of *Chx10* Gi neurons causes ipsilateral movements. **a**, Unilateral infection of *Chx10* Gi neurons with AAV-FLEX-hM3Dq-mCherry. **b**, Turning preference in a cylinder assay 1 h after injection of saline or CNO, quantified as the total number of revolutions over a 10-min trial (**P<0.001; two-way ANOVA with Tukey's multiple comparison test; n=12 mice from three independent experiments). **c**, Movement preference in an open-field assay, quantified between 30 and 60 min after injection of saline or CNO (**P<0.001; two-way ANOVA with Tukey's multiple comparison test; n=12 mice from three independent experiments). Box-and-whisker plots in **b** and **c** give the median, 25th and 75th percentiles, and range. **d**, Instantaneous analysis of movement preference for mice in **c**, quantified as the percentage of ipsilateral versus contralateral revolutions (bin=5 min), after injection of saline (top) or CNO (bottom) at time, t=0. Data are plotted as mean ± s.e.m. **e**, Unilateral injection of AAV-FLEX-ChR2-2A-mCherry into *Chx10^{Cre}* mice. Example of mCherry expression and optical fiber placement in Gi. **f**, Body tracking 1 s before (white), 1 s during (blue) and 1 s after (red) light stimulation. Representative examples are plotted from five different mice (n=7 mice total from two independent experiments). The distance traveled during stimulation is reduced compared with before and after stimulation. **g**, Body center-to-head vectors were plotted as a function of time 0.6 s before (black), 1 s during (blue) and 0.6 s after (red) light stimulation for one representative mouse (n=7 mice in total). **h**, Quantification of movement direction and speed relative to light onset. Photostimulation caused an abrupt shift in movement direction toward the ipsilateral side, accompanied by a reduction in locomotor speed. Gray traces represent the mean for each mouse, whereas the black trace represents the mean calculated across all mice (n=7). **i**, Forty-two individual trials plotted from n=7 mice in two independent experiments, three to nine trials per mouse.

from dorsal horn laminae I–VI where sensory networks are localized, and from lamina IX where motor neurons reside. These data indicate that *Chx10* reticulospinal neurons likely act on premotor networks^{3,12}, rather than on motor neurons themselves¹². We conclude that *Chx10* Gi neurons exhibit mainly ipsilateral projection to the spinal cord, a feature that may allow for differential control of left and right spinal motor networks.

Excitation of *Chx10* Gi neurons causes ipsilateral movements. We next examined the behavioral consequence of unilateral stimulation of *Chx10* Gi neurons in freely moving mice. We expressed excitatory hM3Dq-DREADDs in *Chx10* Gi neurons on one side of the brainstem (Fig. 2a); hM3Dq-DREADDs can be activated with low doses (0.5 mg kg⁻¹) of clozapine-N-oxide (CNO), which causes neuronal depolarization via G_q-mediated signaling³¹. In a cylinder assay, which promotes locomotor turning, we found that CNO administration caused a strong preference in turning toward the side of *Chx10* Gi activation (the ipsilateral side, Fig. 2b). We next examined locomotion in an open field. CNO administration

strongly induced ipsilateral turning even during unrestricted, spontaneous locomotion (Fig. 2c and Supplementary Video 1). CNO administration had no behavioral effect in control mice (Extended Data Fig. 2).

Instantaneous analysis of left-right movement preference in the open field revealed that ipsilateral turning developed over time (Fig. 2d), approaching 100% ipsilateral turning preference by 10 min. At early stages after CNO administration (5–15 min), these ipsilateral turns were smooth—similar to those observed during spontaneous changes in locomotor direction. There were no clear changes in trunk (axial) posture at early stages after administration of CNO. At late stages (>20 min), we observed an ipsilateral axial bend that was evident even at rest (Supplementary Video 1). Notably, during both early and late stages after administration of CNO, we observed changes only in the locomotor direction when the animal started moving forward, suggesting a specific involvement of the limbs. Analysis of locomotor performance in the open field showed that the average speed during locomotor bouts decreased after administration of CNO, with no change in the total distance traveled or the

number of stops per minute (Extended Data Fig. 3a–d). These data indicate that turns are performed during active locomotion without requiring a locomotor arrest (compare with ref. ¹²).

To further investigate the dynamics of this turning behavior, we performed short-lasting photostimulation of *Chx10* Gi neurons after unilateral expression of channelrhodopsin-2 (*Chx10*^{Cre}>AAV-FLEX-ChR2) (Fig. 2e). *Chx10* Gi neurons were stimulated with blue light (473 nm) for 1 s when mice were slowly walking in an open field. Movement trajectories were calculated 1 s before, during and after stimulation (Fig. 2f). In all cases (42 trials in 7 mice), photostimulation led to an abrupt turn toward the ipsilateral side (Fig. 2f and Supplementary Video 2). This ipsilateral turn was initiated within 150 ms, lasted approximately 1.2 s (Fig. 2g,h) and correlated with a reduction in locomotor speed (Fig. 2h,i). Photostimulation at rest could not evoke a locomotor turn, and instead caused head and trunk bending toward the ipsilateral side (Supplementary Video 2).

These experiments suggest that *Chx10* Gi neurons evoke ipsilateral movements via two distinct mechanisms. Stimulation of *Chx10* Gi neurons at rest evoked ipsilateral head/trunk movements, whereas stimulation during ongoing locomotion caused a reduction in locomotor speed accompanied by movements toward the ipsilateral side. *Chx10* Gi neurons appear to encompass all modes of turning; increasing *Chx10* Gi activity caused changes in trunk posture at rest as well as either gradual and/or sharp changes in locomotor direction.

Unilateral inhibition of *Chx10* Gi neurons causes contralateral movements. We next examined the behavioral consequence of unilateral inactivation of *Chx10* Gi neurons using a Cre-dependent tetanus toxin virus (*Chx10*^{Cre}>AAV-FLEX-TeLC-GFP) (Fig. 3a). In the cylinder assay, we found that FLEX-TeLC-injected (but not FLEX-GFP-injected) mice exhibited a strong turning preference toward the contralateral side (Fig. 3b). We performed a time-course analysis of turning preference after TeLC injection in the open field. A day before injection of FLEX-TeLC-GFP or FLEX-GFP, mice exhibited no open-field turning preference (Fig. 3c,d and Supplementary Video 3). Mice injected unilaterally with FLEX-TeLC (but not FLEX-GFP) started to exhibit turning contralateral to the injected side as soon as 3 d after injection (Fig. 3c,d). By 9 d, 100% of TeLC mice exhibited contralateral turning (Fig. 3c,d and Supplementary Video 3). Early after TeLC injection, contralateral turns were smooth and there were no obvious effects on trunk posture at rest (Supplementary Video 3). When the phenotype had fully developed at days 6–9, turns were sharper than in the early stages (Supplementary Video 3). Therefore, similar to unilateral *Chx10* Gi stimulation, inhibition of *Chx10* Gi activity caused both gradual and sharp modes of locomotor turning, but toward the contralateral side. To substantiate these results, we also performed acute inactivation of *Chx10* Gi neurons using inhibitory DREADDS (*Chx10*^{Cre}>FLEX-hM4Di). Similar to chronic inactivation of *Chx10* Gi neurons, acute inactivation promoted contralateral locomotor turning (Fig. 3e–h).

Unilateral inactivation of *Chx10* Gi neurons increased the speed and total distance mice moved during a 30-min probe (Extended Data Fig. 3e–h). There was, however, no change in the number of stops per minute (Extended Data Fig. 3). These data suggest that *Chx10* Gi neurons act as a unilateral ‘brake’ on locomotion, and removing this unilateral brake increases locomotor speed and number of turns toward the contralateral side.

Differential control of left-right spinal motor networks. We next asked whether ipsilateral projection of *Chx10* Gi neurons can allow for differential control of left and right spinal motor networks using an in vitro split-bath preparation (Fig. 4a). Locomotor-like hindlimb activity is maintained by adding locomotor-promoting drugs NMDA and/or serotonin and 5-hydroxytryptamine (5HT)

(sometimes with dopamine) to the lumbar spinal cord while excitatory synaptic activity is blocked in the brainstem (with the broadly acting glutamate receptor blocker, kynurenic acid) (Fig. 4a). Stimulating *Chx10* Gi neurons in this configuration excludes the possibility that locomotor effects are due to axon collaterals acting on local networks in the brainstem^{12,32}. In *Chx10*^{Cre};R26R^{ChR2} preparations, we found that unilateral stimulation of *Chx10* Gi neurons with blue light could not evoke a response in lumbar roots. In contrast, during drug-induced locomotor activity, stimulation could decrease the frequency and/or the amplitude of flexor-related rhythmic hindlimb locomotor activity on the side ipsilateral to stimulation (Ipsi L2, corresponding to reduced swing-phase activity), with little effect on the contralateral side (Contra L2) (Fig. 4b–g; n=7, 52 trials). The extensor-related locomotor burst activity on the ipsilateral side (Ipsi L5) was prolonged, which corresponds to an increased stance duration (Extended Data Fig. 4a–e; n=4, 33 trials). These observations phenocopy data demonstrating that rhythmicity can be controlled unilaterally in the cord^{23,33}, and suggest a strong inhibitory effect on rhythm-generating locomotor circuits in the lumbar cord (see also ref. ¹²).

The dominant inhibitory effect on hindlimb locomotor rhythrogenesis by *Chx10* Gi stimulation suggests that the descending excitatory signal acts on inhibitory spinal neurons, as previously demonstrated by anterograde tracing¹². To test this more directly, we blocked inhibitory transmission in the spinal cord using picrotoxin (PTX), a GABA_A-receptor and partial glycinergic-receptor blocker. In the presence of PTX (10 μM), the ipsilateral inhibitory effect was blocked (n=5, 69 trials), and sometimes sign reversed such that stimulation caused L2/L5 excitation (no inhibition; Extended Data Fig. 5a–c). In contrast to the inhibitory effect observed at the lumbar level, unilateral stimulation of *Chx10* Gi neurons caused excitation of thoracic motor neurons that control axial musculature (Extended Data Fig. 5b; n=4, 46 trials), which was PTX insensitive (Extended Data Fig. 5c). We conclude that *Chx10* Gi neurons can function as a unilateral locomotor effector via unilateral inhibition of locomotor rhythrogenesis. At the thoracic level, however, *Chx10* Gi neurons cause excitation of axial motor neurons.

To investigate this further, we performed in vivo experiments with electromyography (EMG) in lightly anesthetized mice. Unilateral *Chx10* Gi stimulation caused a dominant contraction of ipsilateral axial muscles (Fig. 4h–k), including splenius capitis (latency of 14.6±1.0 ms, n=5, ipsilateral head turn) and external abdominal oblique (latency of 23.2±1.7 ms, n=3, ipsilateral trunk bend). In all cases, the dominant movement produced by the stimulus was toward the ipsilateral side; however, in three mice there was a negligible EMG response on the contralateral side as well (Fig. 4i,j). Axial muscle activation appeared to be mediated by *Chx10* Gi activation of spinal excitatory neurons (a polysynaptic response) rather than direct monosynaptic activation of motor neurons; axial motor unit recruitment was variable in response to the same stimulus strength and did not follow a high-frequency train of stimuli with consistent spiking (Fig. 4k). In stark contrast to the excitation of axial muscles, we did not observe any responses from hindlimb flexors or extensors recorded at the same time (Fig. 4h,k). Together the in vitro and in vivo results indicate a dual effect of ipsilateral *Chx10* Gi activation: ipsilateral excitation of axial muscles (through local excitatory neurons) and ipsilateral inhibition of rhythmic locomotor activity (through local inhibitory neurons).

Limb dynamics during natural and drug-evoked turns. Our data suggest that the mechanism for *Chx10*-evoked locomotor turns reflects distinct changes in limb dynamics: *Chx10*-evoked ipsilateral turns were accompanied by a decrease in locomotor speed (Fig. 3f,g and Extended Data Fig. 3a), whereas inhibition of *Chx10* Gi neurons caused contralateral turning accompanied by an increase in overall locomotor speed (Extended Data Fig. 3e).

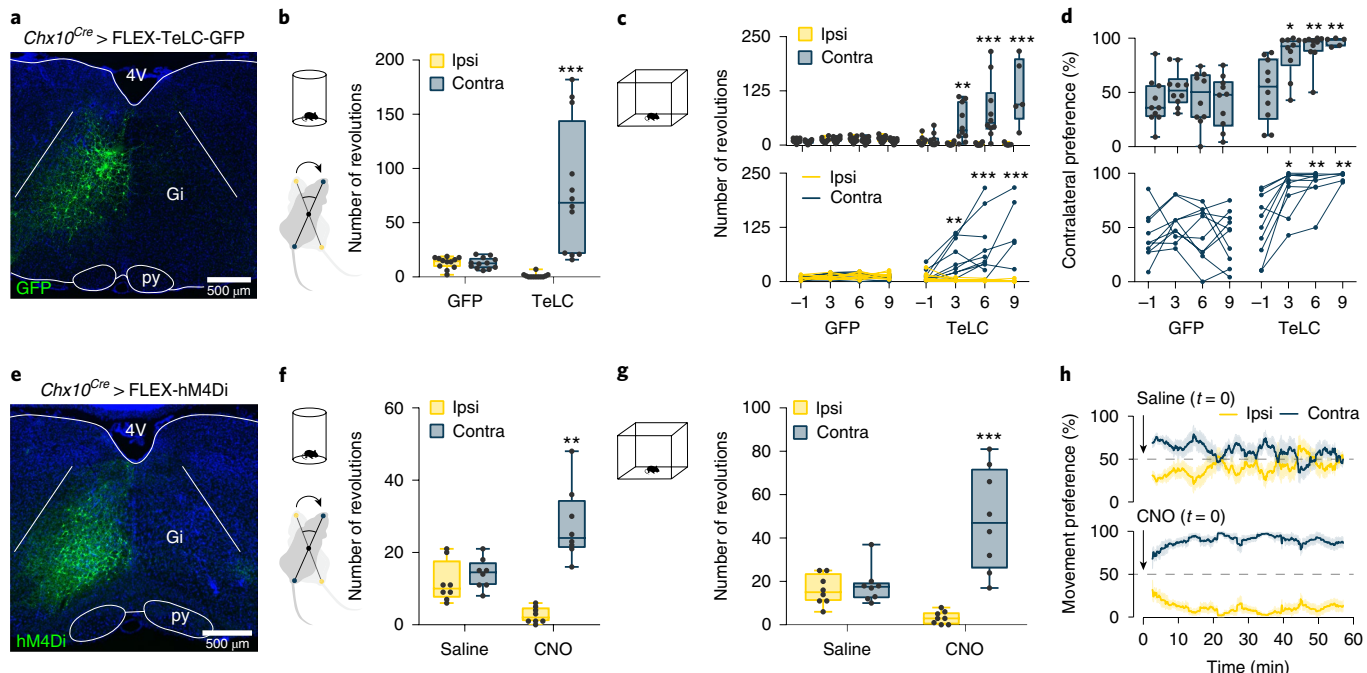


Fig. 3 | Inhibition of *Chx10* Gi neurons causes contralateral movements. **a**, Unilateral injection of AAV-FLEX-TeLC-GFP or AAV-FLEX-GFP in *Chx10^{Cre}* mice. Example of GFP expression in Gi 2 weeks after injection. **b**, Turning preference in a cylinder assay 7 d after viral injection, quantified as the total number of revolutions over a 10-min trial (**P < 0.001; two-way ANOVA with Tukey's multiple comparison test; n = 12 mice from three independent experiments). **c**, Turning preference in an open-field assay, quantified as the total number of revolutions during a 30-min trial (**P = 0.0046, day 3 TeLC Ipsi versus Contra; ***P < 0.001, day 6 TeLC Ipsi versus Contra; ***P < 0.001, day 9 TeLC Ipsi versus Contra) (Supplementary Table 1). Three-way ANOVA with Tukey's multiple comparison test; n = 10 mice from two independent experiments for GFP days -1, 3, 6 and 9; n = 10 mice from two independent experiments for TeLC days -1, 3 and 6; n = 5 mice for TeLC day 9. The top panel gives the box-and-whisker distribution for each group, whereas the bottom panel gives the phenotypic progression in each animal. **d**, Turning preference in an open-field assay, quantified as the percentage of total revolutions during a 30-min trial (*P = 0.0211, day 3 versus day -1 TeLC; **P = 0.003, day 6 versus day -1 TeLC; **P = 0.0067, day 9 versus day -1 TeLC; two-way ANOVA with Tukey's multiple comparison test; n = 10 mice for GFP days -1, 3, 6 and 9; n = 10 mice for TeLC days -1, 3 and 6; n = 5 mice for TeLC day 9) (Supplementary Table 1). Box-and-whisker plots in **b-d** give the median, 25th and 75th percentiles, and range. **e**, Example of hM4Di expression after unilateral injection of AAV-FLEX-hM4Di in *Chx10^{Cre}* mice. **f**, Turning preference in a cylinder assay 20 min after injection of saline or CNO, quantified as the total number of revolutions over a 10-min trial (**P = 0.0011; two-way ANOVA with Tukey's multiple comparison test; n = 8 mice from two independent experiments). **g**, Turning preference in an open-field assay, quantified between 30 and 60 min after injection of saline or CNO (**P < 0.001; two-way ANOVA with Tukey's multiple comparison test; n = 8 mice from two independent experiments). Box-and-whisker plots in **f** and **g** give the median, 25th and 75th percentiles, and range. **h**, Instantaneous analysis of movement preference for mice in **g**, quantified as the percentage of ipsilateral versus contralateral revolutions (bin = 5 min), after injection of saline (top) or CNO (bottom) at t = 0. Data are plotted as mean ± s.e.m.

To investigate these limb dynamics in greater detail, we analyzed how limb coordination relates to locomotor direction in freely moving mice. DeepLabCut was used for markerless extraction of forelimb and hindlimb paw position in an open field (Supplementary Video 4)³⁴. We focused on continuous locomotor bouts with a speed >5 cm s⁻¹, which corresponds to walk or trot³⁵. For locomotor bouts in wild-type (WT) mice, locomotion that proceeded in a straight line exhibited a similar stride length on the left and right sides (Fig. 5a). During spontaneous turns, stride length was reduced on the side of the turn (Fig. 5a). This was true for both the forelimbs and the hindlimbs. We compared spontaneous turns in WT mice with those biased to one side via excitation (*Chx10^{Cre}* > hM3Dq-DREADDs after CNO) or inhibition (*Chx10^{Cre}* > FLEX-TeLC) of *Chx10* Gi neurons (Fig. 5b,c). Turns in WT mice and those caused by *Chx10^{Cre}* > FLEX-hM3Dq or *Chx10^{Cre}* > FLEX-TeLC shared a defining characteristic, that is, the hindlimbs and the forelimbs on the side of the turn traveled a shorter distance than the leg opposite to the turn (Fig. 5b,c).

We next asked whether differences in stride length between the left and right sides were sufficient to predict locomotor direction (Fig. 5d). For this we examined the relationship between the distance traveled by the right and left limbs and heading direction

for all locomotor bouts sampled in WT, *Chx10^{Cre}* > FLEX-hM3Dq and *Chx10^{Cre}* > FLEX-TeLC mice. In WT mice, we observed epochs with no difference in left-right stride length, which corresponded to straight walking, as well as epochs with longer left leg steps (turning right) and longer right leg steps (turning left). *Chx10^{Cre}* > FLEX-hM3Dq mice exhibited shorter steps on the side of injection, which caused ipsilateral turns. *Chx10^{Cre}* > FLEX-TeLC mice exhibited longer steps on the side of injection, which caused contralateral turns (Fig. 5e,f and Extended Data Fig. 6a-d). Together these data lead to a model where the difference in stride length on the left and right sides predicts locomotor direction ($r^2 = 0.96$ for absolute distance, Fig. 5e; $r^2 = 0.95$ for log₂(ratio), Fig. 5f). These data are compatible with the hypothesis that increased *Chx10* Gi activity reduces the amplitude of locomotor bursts on the ipsilateral side (as observed in vitro), leading to shorter steps on the side of the turn.

***Chx10* Gi neurons are required for turning during exploration.** To test the necessity of *Chx10* Gi neurons for turns during natural exploratory behaviors, we designed a paradigm in which mice explored a left- or right-turned maze (Fig. 6a). Mice were placed in the center of this simple spiral-shaped maze, which

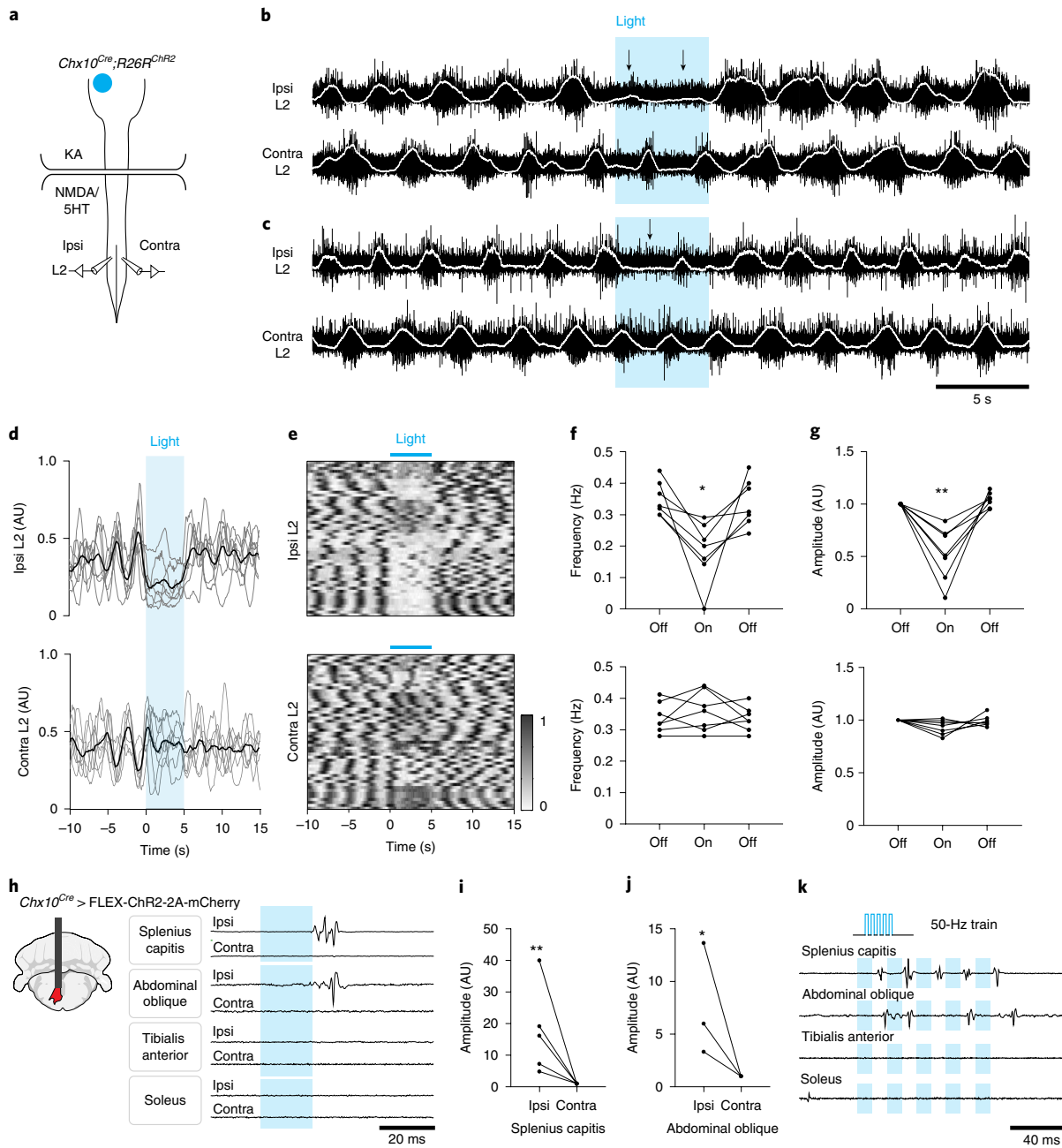


Fig. 4 | Chx10 Gi neurons cause inhibition of ipsilateral rhythmic locomotor activity and excitation of ipsilateral axial muscles. **a**, Schematic of split-bath brainstem-spinal cord preparation from P0–4 *Chx10^{Cre};R26R^{ChR2}* mice, which was used to interrogate unilateral function of *Chx10* Gi neurons in vitro. A rostral brainstem compartment was bathed with kynurenic acid (KA, 4 mM) to block all glutamatergic transmission among axon collaterals³², and a caudal spinal cord compartment was bathed with NMDA (6–8 μM) and serotonin (5HT, 5–15 μM) (sometimes with dopamine, 50–100 μM) to induce locomotor-like activity, assayed by recording from the L2 ventral roots. **b,c**, Unilateral photostimulation of *Chx10* Gi neurons reduced the frequency (**b**) and/or amplitude (**c**) of locomotor-like activity ipsilateral (Ipsi L2) to stimulation, with little effect on the contralateral side (Contra L2). Traces in **b** and **c** are derived from two different mice and represent $n=7$ independent preparations. **d**, Integrated traces normalized in amplitude from 0 to 1 and averaged across trials for each mouse ($n=7$ mice, gray), with the grand average across mice represented in black. AU, arbitrary units. **e**, From 7 mice, 52 trials represented as intensity plots from 0 to 1, which are integrated traces normalized from 0 to 1. Three of the mice represented for Ipsi L2 are also represented in Extended Data Fig. 4. **f**, Quantification of Ipsi L2 and Contra L2 frequency in response to photostimulation (* $P=0.021$; $n=7$ mice; one-way repeated measures ANOVA, light-on versus baseline). **g**, Quantification of Ipsi L2 and Contra L2 amplitude in response to photostimulation (** $P=0.0063$; $n=7$ mice; one-way repeated measures ANOVA, light-on versus baseline). **h**, Schematic of fiber placement in the Gi after injection of AAV-FLEX-ChR2-2A-mCherry in *Chx10^{Cre}* mice. EMG signals were recorded in axial muscles (splenius capitis or abdominal oblique) and/or hindlimb flexor (tibialis anterior) and extensor (soleus) muscles on the left and right sides of the body. Strong EMG responses could be evoked in the ipsilateral splenius capitis muscle ($n=5$ mice) and abdominal oblique muscle ($n=3$ mice). No responses were observed in the hindlimb flexor (tibialis) or extensor (soleus) muscles ($n=3$ mice). **i**, Quantification of the peak-to-peak response amplitude in the ipsilateral and contralateral splenius capitis muscles (** $P=0.0022$; ratio paired, two-tailed Student's *t*-test; $n=5$ mice). **j**, Quantification of the response amplitude in the ipsilateral and contralateral abdominal oblique (* $P=0.0446$; ratio paired, two-tailed Student's *t*-test; $n=3$ mice). **k**, Responses in splenius capitis and abdominal oblique to a high-frequency (50 Hz) stimulus train were variable. Motor units did not follow the stimulus train, suggesting a polysynaptic connection between *Chx10* Gi neurons and motor neurons. Traces in **k** represent $n=3$ mice for each muscle.

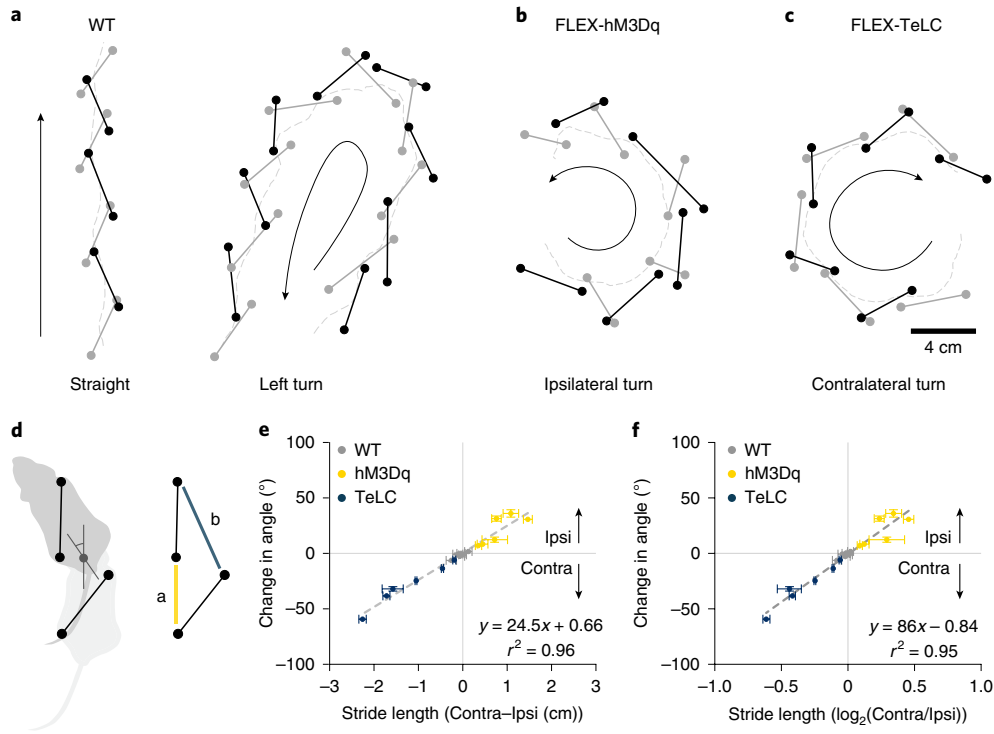


Fig. 5 | Limb dynamics during natural and *Chx10*-induced turns. **a**, Representative examples of footfalls in a WT mouse walking straight and making a spontaneous left turn ($n=6$ mice from one experiment). Black lines indicate the left-forelimb/right-hindlimb diagonal, whereas gray lines indicate the right-forelimb/left-hindlimb diagonal. For spontaneous turns, the limb on the side of the turn exhibits shorter steps than its corresponding diagonal. **b**, Representative example of footfalls in a left *Gi Chx10^{Cre}*> FLEX-hM3Dq mouse after injection of CNO ($n=6$ mice from two independent experiments), which causes turning toward the ipsilateral (left) side. **c**, Representative example of footfalls in a left *Gi Chx10^{Cre}*> FLEX-TeLC mouse ($n=6$ mice from two independent experiments), which causes turning toward the contralateral (right) side. Steps are longer on the ipsilateral side. **d**, Schematic of turning based on data in **a–c**. A single step can exhibit left-right motor asymmetry, where the ipsilateral hindlimb exhibits a shorter stride length (**a**) than the diagonal limb of the contralateral side (**b**), leading to changes in heading position. **e,f**, Mathematical models demonstrating that a difference in stride length predicts a difference in heading position. We quantified footfalls in WT ($n=6$ mice from one experiment), *Chx10^{Cre}*> FLEX-hM3Dq (hM3Dq) ($n=6$ mice from two independent experiments) and *Chx10^{Cre}*> FLEX-TeLC (TeLC) ($n=6$ mice from two independent experiments) mice. For WT mice, the difference in stride length, measured as either the absolute distance (**e**) or the \log_2 (ratio) (**f**), was close to zero, corresponding to straight walking and/or slight turning to one side. For FLEX-hM3Dq mice after CNO injection, the values are positive—predicting an ipsilateral turn. For FLEX-TeLC mice, the values are negative—predicting a contralateral turn (** $P < 0.001$ for regression in **e** and **f**; F -test; $n=18$ mice). Data points in **e** and **f** are plotted as mean \pm s.e.m. Vertical error bars are omitted in cases where the s.e.m. is smaller than the data point itself. Goodness of fit is given as the coefficient of determination (r^2 , the square of Pearson's r).

they explored until they exited the maze or 10 min had elapsed. Unaffected mice rapidly completed both left- and right-turned mazes (Fig. 6a–d). In contrast, unilateral activation of *Chx10* Gi neurons with hM3Dq-DREADDs increased exploratory time in a contralateral but not an ipsilateral maze (Fig. 6a,b), with several mice failing to complete the contralateral maze altogether ($n=6/8$, Fig. 6b). Mirroring this effect, inactivation of *Chx10* Gi neurons with TeLC increased exploratory time in an ipsilateral but not a contralateral maze (Fig. 6c), with several mice failing to complete the ipsilateral maze ($n=3/8$, Fig. 6d). These experiments show that mice do not have an ability to compensate for dysfunction of the *Chx10* turning system, which appears to be required for natural exploratory function.

Contralateral superior colliculus steering acts through *Chx10* Gi neurons. These experiments define a final command pathway for executing left-right locomotor asymmetries. The remaining question is whether it is possible to recruit *Chx10* Gi neurons unilaterally during natural behaviors. To address this question, we first performed monosynaptically restricted, transsynaptic labeling from *Chx10* Gi neurons to determine their immediate synaptic inputs^{36,37}. Cre-dependent rabies helper virus (AAV-FLEX-helper;

see Methods) was injected in the left *Gi* of *Chx10^{Cre}* mice, followed by RVΔG-4mCherry(EnvA). Consistent with our results using anterograde tracing (Fig. 1b), monosynaptic retrograde tracing demonstrated that *Chx10* Gi neurons do not exhibit strong connectivity across the midline (Extended Data Fig. 7b,c); *Chx10* Gi neuronal populations are not reciprocally connected. *Chx10* Gi neurons received long-range, primarily unilateral inputs from the contralateral superior colliculus (SC), the ipsilateral zona incerta, the ipsilateral mesencephalic reticular formation (mRt) and the contralateral medial cerebellar (fastigial) nucleus (Fig. 7a, Extended Data Fig. 7 and Supplementary Table 2). *Chx10* Gi neurons also exhibited bilateral long-range inputs from the lateral cerebellar (the dentate) nuclei and sensorimotor cortex (Extended Data Fig. 7 and Supplementary Table 2). Notably, no transsynaptic labeling was observed from the cuneiform or pedunculopontine nuclei, which comprise the midbrain locomotor region (Supplementary Table 2). These experiments provide anatomic evidence that activity of *Chx10* Gi neurons can be biased via unilateral input from upstream nuclei.

To test this possibility we stimulated the SC-Gi projection. We focused on the SC because of its prominent role in sensorimotor integration^{38–40}, and for its role in gaze and head orientation within

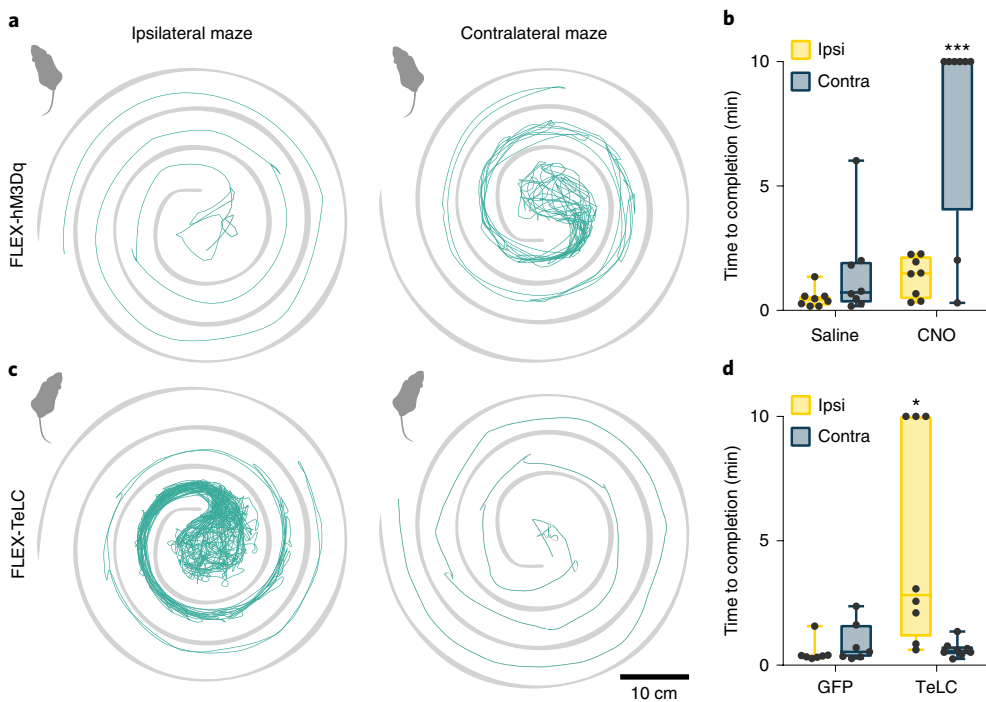


Fig. 6 | Unilateral function of *Chx10* Gi neurons is critical for left-right movements during natural exploratory behaviors. **a**, Activation of *Chx10* Gi neurons unilaterally with excitatory hM3Dq-DREADDs impairs exploration in a contralateral (right-turn) maze. Turquoise traces represent the movement trajectory of a single representative mouse—the same mouse is represented in both the ipsilateral and the contralateral mazes. **b**, Six of eight CNO-injected mice failed to complete the contralateral maze during a 10-min trial (**P < 0.001; two-way ANOVA with Tukey's multiple comparison test; n = 8 mice from one experiment). **c**, Inhibition of *Chx10* Gi neurons unilaterally with TeLC impairs exploration in an ipsilateral (left-turn) maze. **d**, Three of eight TeLC-injected mice failed to complete the ipsilateral maze during a 10-min trial (*P = 0.011; two-way ANOVA with Tukey's multiple comparison test; n = 7 mice for GFP and n = 8 mice for TeLC (one experiment)). Box-and-whisker plots in **b** and **d** give the median, 25th and 75th percentiles, and range.

three-dimensional space⁴¹. Projections from the contralateral SC to the Gi have been described³⁸. We now show that these SC–Gi projection neurons occupy intermediate layers of the SC, and they synapse specifically with *Chx10* Gi neurons (Fig. 7a,b). We tested the behavioral significance of this SC–Gi projection in four different ways. First, the SC–Gi projection was targeted by retrograde labeling of SC neurons using $Gi_{ipsi} > AAV_{retro}$ -Cre, followed by $SC_{contra} > FLEX-hM3Dq$ (Fig. 7c). SC neurons targeted using this approach had a discrete laminar position that matched the rabies transsynaptic tracing (Fig. 7a,c). In these mice, CNO administration rapidly initiated ipsilateral turning (Fig. 7d). Next, postsynaptic Gi neurons were targeted using $SC_{contra} > AAV1$ -Cre, an anterograde transsynaptic virus³⁸, followed by $Gi_{ipsi} > FLEX-hM3Dq$ (Fig. 7e). Gi neurons exhibited robust recombination on the ipsilateral side (Fig. 7e). Again, CNO administration rapidly initiated ipsilateral turning (Fig. 7f).

We supplemented these approaches using an intersectional strategy to allow both projection- and target-specific recombination (Fig. 7g–j). In *Chx10*^{Cre} mice, targeting postsynaptic Gi neurons using $SC_{contra} > AAV1$ -FLEX-FlpO followed by $Gi_{ipsi} > dFRT-hM3Dq$, caused recombination in ipsilateral *Chx10* Gi neurons (Fig. 7g). CNO administration rapidly initiated ipsilateral turning (Fig. 7h). Finally, we showed that the SC–Gi projection neurons are glutamatergic. In *Vglut2*^{Cre} (*Slc17a6*) mice⁴², glutamatergic SC–Gi projection neurons were targeted using $Gi_{ipsi} > AAV_{retro}$ -FLEX-FlpO followed by $SC_{contra} > dFRT-hM3Dq$ (Fig. 7i). CNO administration rapidly initiated ipsilateral turning (Fig. 7j). These results show that a natural sensorimotor pathway can bias *Chx10* Gi neuronal activity during spontaneous locomotion. Moreover, these experiments unambiguously demonstrate that the SC imparts left-right locomotor directional commands via *Chx10* Gi neurons.

Discussion

The present study uncovers a command system that enables left-right locomotor asymmetries necessary for directional movements. This asymmetric reticulospinal command system functions in parallel with symmetric start and speed control circuits^{7–9,11}, and may be used symmetrically to arrest ongoing locomotion¹². Our study, therefore, completes the description of the three main requisite control components for locomotion: start, stop and direction. Remarkably, when *Chx10* Gi neurons were biased to produce either ipsilateral or contralateral movements, mice could not perform a compensatory turn. This observation suggests that the turning system revealed here is the dominant system used during natural behaviors, and is recruited by brain circuits involved in mediating directional movements.

Mechanism for locomotor turns. In aquatic vertebrates, left–right steering movements are achieved by asymmetric activity of glutamatergic reticulospinal neurons on the left and right sides. This causes a forceful contraction of axial muscles on the side of the turn^{43–46}. In our experiments, we show that asymmetric movements in mice are also caused by an imbalance in descending excitation between the left and right sides, which has a dual effect on spinal circuits—unilateral *Chx10* Gi neuronal activity: (1) causes contraction of the ipsilateral axial muscles and bending of the trunk on the ipsilateral side, and (2) suppresses ipsilateral flexor-related locomotor activity that promotes ipsilateral turning by reducing stride length (force generation) on the ipsilateral side. Thus, excitation in spinal limb locomotor circuits is reduced on the side of the turn.

In previous studies we have shown that bilateral activation of *Chx10* Gi neurons arrests or reduces limbed locomotor activity via a brake on locomotor rhythmogenesis in the cord¹². In the

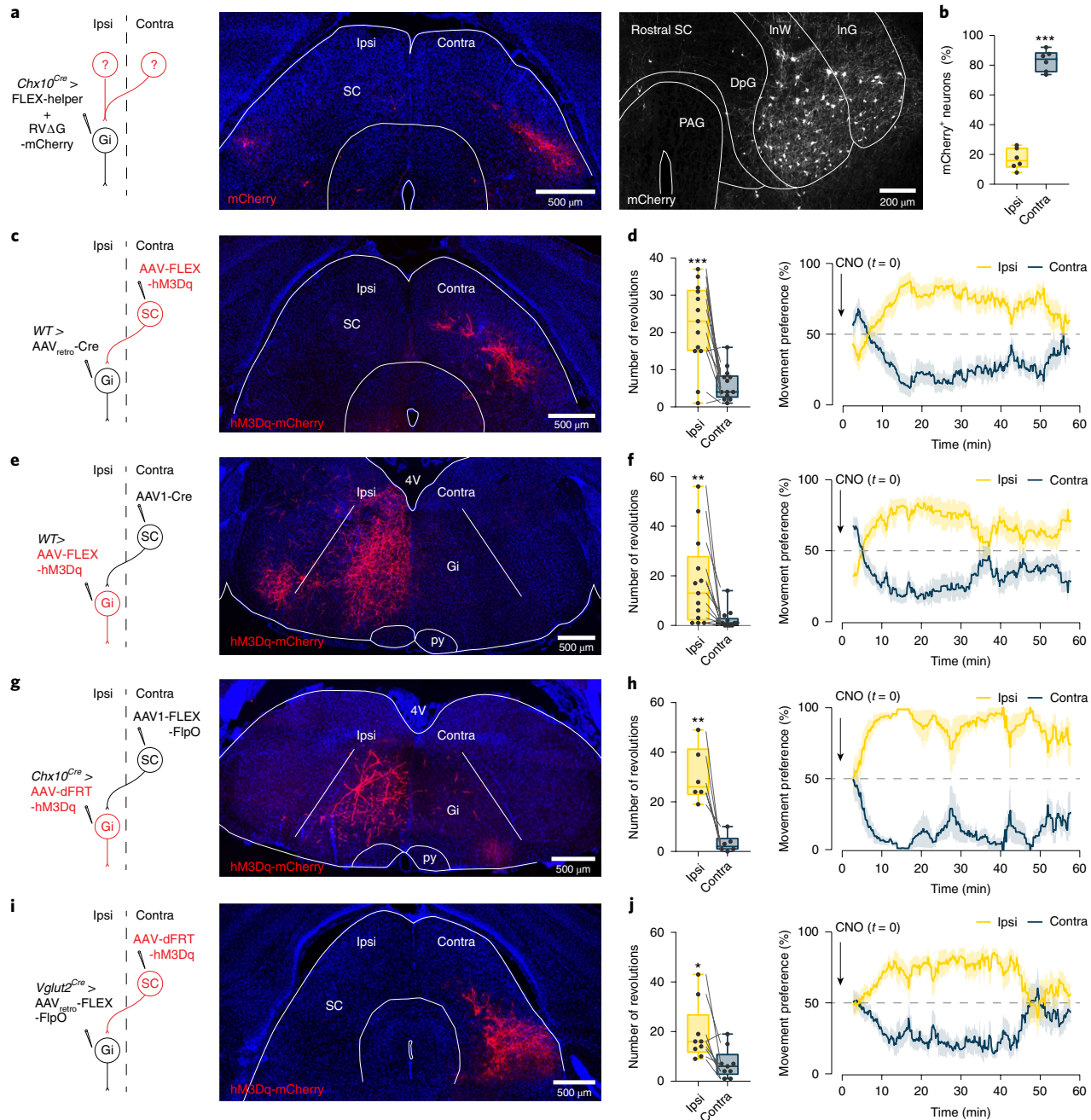


Fig. 7 | Contralateral SC steering acts through *Chx10* Gi neurons. **a**, A rabies transsynaptic tracing approach was used to identify presynaptic inputs to *Chx10* Gi neurons (Extended Data Fig. 7 and Supplementary Table 2). Rabies-mCherry tracing revealed a prominent input from the contralateral SC, where neurons occupied intermediate layers (left, caudal SC; right, rostral SC). **b**, Quantification of mCherry-labeled neurons in the ipsilateral and contralateral SC (***P* < 0.001; paired, two-tailed Student's *t*-test; *n* = 6 mice from one experiment). **c**, Retrograde behavioral interrogation of the SC-Gi synapse in WT mice. Injection of AAV_{retro}-Cre in the Gi caused recombination of a FLEX-hM3Dq-mCherry virus injected into the contralateral SC (*n* = 13 mice). **d**, CNO injection caused an ipsilateral turning preference (***P* = 0.0004; paired, two-tailed Student's *t*-test; *n* = 13 mice from two independent experiments). Right: instantaneous quantification of turning percentage after CNO injection. **e**, Anterograde behavioral interrogation of the SC-Gi synapse in WT mice. Injection of AAV1-Cre into the contralateral SC caused recombination of a FLEX-hM3Dq-mCherry virus injected into the ipsilateral Gi (*n* = 13 mice). **f**, CNO injection caused an ipsilateral turning preference (***P* = 0.0087; paired, two-tailed Student's *t*-test; *n* = 13 mice from two independent experiments). Right: instantaneous quantification of turning percentage after CNO injection. **g**, Anterograde behavioral interrogation of the SC-Gi synapse in *Chx10^{Cre}* mice. Injection of AAV1-FLEX-FlpO into the contralateral SC caused recombination of a dFRT-hM3Dq-mCherry virus injected in the ipsilateral Gi (*n* = 6 mice). **h**, CNO injection caused an ipsilateral turning preference (***P* = 0.0053; paired, two-tailed Student's *t*-test; *n* = 6 mice from two independent experiments). Right: instantaneous quantification of turning percentage after CNO injection. **i**, Retrograde behavioral interrogation of the SC-Gi synapse in *Vglut2^{Cre}* mice. Injection of AAV_{retro}-FLEX-FlpO into the Gi caused recombination of a dFRT-hM3Dq-mCherry virus injected into the contralateral SC (*n* = 9 mice). **j**, CNO injection caused an ipsilateral turning preference (**P* = 0.0113; paired, two-tailed Student's *t*-test; *n* = 9 mice from two independent experiments). Right: instantaneous quantification of turning percentage after CNO injection. Box-and-whisker plots in **b**, **d**, **f**, **h** and **j** give the median, 25th and 75th percentiles, and range. Time-series data in **d**, **f**, **h** and **j** are plotted as mean \pm s.e.m.

present study we show that unilateral stimulation of *Chx10* Gi neurons reduces the frequency and/or amplitude of flexor-related hindlimb locomotor activity with a simultaneous prolongation of extensor-related activity. This effect can be observed only during active locomotion and is suppressed by blocking inhibitory synaptic transmission in the cord. In contrast, unilateral *Chx10* Gi activity leads to activation of axial muscles, observed even at rest, which is insensitive to blockade of inhibitory synaptic transmission in the cord. The mechanisms for these opposing effects, therefore, appear to reflect differential engagement of spinal premotor networks: At the limb level *Chx10* Gi neurons appear to preferentially engage ipsilateral inhibitory networks, whereas at the axial level *Chx10* Gi neurons appear to preferentially engage ipsilateral excitatory networks.

The unilateral *Chx10* Gi gain- and loss-of-function experiments demonstrate that a unilateral brake (activation of *Chx10* Gi neurons) or release of the brake (inactivation of *Chx10* Gi neurons) is essential for mediating a limb-based turn—where speed and stride length are higher on the side opposite to the turn. The reduction in frequency and/or amplitude of flexor-related activity and corresponding prolongation of extensor-related activity observed *in vitro* corresponds well with unilateral changes in step length observed *in vivo*. In many instances, stride length is shortened and locomotor turning is achieved without significant axial bending, which suggests that limb perturbation is a determining factor. Indeed, there is no evidence that axial bending alone is sufficient to initiate a turn as observed in aquatic vertebrates.

We suggest that this turning mechanism for limbed species evolved to account for general features of the limbed body plan. Chiefly, axial muscles generate force perpendicular to the directional axis. In contrast, limbs generate force parallel to the directional axis but at a distance from the midline, creating a moment about the medial axis. Although locomotor direction is ultimately mediated by the limbs and requires locomotion⁴⁷, unilateral stimulation of *Chx10* Gi neurons also evoked bending of the head and trunk toward the side of stimulation, even at rest. Based on these observations we propose that limbed animals use a two-component system for directing movements to the left or right side. Perhaps not surprisingly, this two-component biological turning system is a design principle adopted for steering four-wheeled vehicles millions of years after it was selected during evolution to control left–right locomotor asymmetries in quadrupeds: turning in quadrupeds and four-wheeled vehicles is enabled by a dedicated steering/differential system for independent control of speed on the left and right sides.

Comparisons with brainstem *Chx10* neurons in aquatic animals. Interestingly, *Chx10* reticulospinal neurons project unilaterally in zebrafish⁴⁸, and unilateral ablation of *Chx10* ventral brainstem, spinal projection neurons (including nuclei RoV3, MiV1 and MiV2) impairs visually guided and spontaneous turns⁴⁴. Calcium imaging of these *Chx10* spinal projection neurons revealed that their activity strongly correlated with activity on the side of the turn—that is, on the side of axial muscle contraction. Thus, remarkably, zebrafish and mice both use *Chx10* reticulospinal neurons to transform forward locomotor bouts into movements toward the ipsilateral side. Based on these data, we propose that *Chx10* (Gi) reticulospinal neurons act as a phylogenetically preserved system for imparting directional locomotor commands in all vertebrate species.

Integrated function of *Chx10* Gi neurons. Mammalian *Chx10* Gi neurons were initially associated with locomotor stop, a behavioral response caused by bilateral activation¹². The data presented in the present study give clear evidence that asymmetric engagement of *Chx10* Gi neurons causes turning. *Chx10* Gi neurons may therefore have a dual function—stop or turn—dependent on their symmetric or asymmetric activation. The basis for differential engagement may rest in task-dependent recruitment from upstream brain areas.

Accordingly, our rabies tracing screen demonstrated that certain presynaptic nuclei contribute prominent bilateral or unilateral input. Prominent bilateral inputs from the lateral deep cerebellar nuclei and sensorimotor cortex (among others) provide an anatomic basis for a symmetric stop command. Prominent unilateral input from neurons in the intermediate layers of the contralateral SC, the ipsilateral zona incerta, the ipsilateral mRt and the fastigial nucleus provide a basis for recruiting an asymmetric turn command. Indeed, we demonstrate that activation of the crossed SC–*Chx10* Gi pathway mediates movements contralateral to the SC. These experiments clearly demonstrate that *Chx10* Gi neurons can be recruited to generate locomotor asymmetries through the SC, a hub for sensorimotor integration^{38,41}.

Interestingly, the SC, zona incerta and mRt were recently identified in a brain-wide screen for neurons that control the decision to move left or right²². Furthermore, it has been shown that glutamatergic fastigial neurons project to the contralateral Gi⁴⁹. Our present brain-wide screen links this excitatory cerebellar output to *Chx10* Gi neurons. Fastigial neurons are downstream of the vestibule cerebellum, which has been shown to encode turning during locomotion⁵⁰. Glutamatergic inputs from contralateral SC and fastigial neurons to *Chx10* Gi neurons, therefore, contribute information from both sensorimotor and vestibular sources, information that ultimately biases locomotor movements to the ipsilateral side.

Together our findings suggest that *Chx10* Gi neurons act as the final common effector for left–right movements, and might act as a locus for integration of diverse sensorimotor signals, which contribute to the decision to move left or right. Understanding the specific contribution of brain areas upstream of *Chx10* Gi neurons—and how they work in concert—is expected to lead to a more thorough understanding of how motor control is organized at the behavioral level.

Online content

Any methods, additional references, Nature Research reporting summaries, source data, extended data, supplementary information, acknowledgements, peer review information; details of author contributions and competing interests; and statements of data and code availability are available at <https://doi.org/10.1038/s41593-020-0633-7>.

Received: 2 September 2019; Accepted: 31 March 2020;

Published online: 11 May 2020

References

- Grillner, S. The motor infrastructure: from ion channels to neuronal networks. *Nat. Rev. Neurosci.* **4**, 573–586 (2003).
- Kiehn, O. Decoding the organization of spinal circuits that control locomotion. *Nat. Rev. Neurosci.* **17**, 224–238 (2016).
- Goulding, M. Circuits controlling vertebrate locomotion: moving in a new direction. *Nat. Rev. Neurosci.* **10**, 507–518 (2009).
- Brownstone, R. M. & Wilson, J. M. Strategies for delineating spinal locomotor rhythm-generating networks and the possible role of Hb9 interneurones in rhythrogenesis. *Brain Res. Rev.* **57**, 64–76 (2008).
- Jordan, L. M., Liu, J., Hedlund, P. B., Akay, T. & Pearson, K. G. Descending command systems for the initiation of locomotion in mammals. *Brain Res. Rev.* **57**, 183–191 (2008).
- Ryczko, D. & Dubuc, R. The multifunctional mesencephalic locomotor region. *Curr. Pharm. Des.* **19**, 4448–4470 (2013).
- Capelli, P., Pivetta, C., Soledad Esposito, M. & Arber, S. Locomotor speed control circuits in the caudal brainstem. *Nature* **551**, 373–377 (2017).
- Caggiano, V. et al. Midbrain circuits that set locomotor speed and gait selection. *Nature* **553**, 455–460 (2018).
- Josset, N. et al. Distinct contributions of mesencephalic locomotor region nuclei to locomotor control in the freely behaving mouse. *Curr. Biol.* **28**, 884–901.e3 (2018).
- Musienko, P. E. et al. Spinal and supraspinal control of the direction of stepping during locomotion. *J. Neurosci.* **32**, 17442–17453 (2012).
- Roseberry, T. K. et al. Cell-type-specific control of brainstem locomotor circuits by basal ganglia. *Cell* **164**, 526–537 (2016).

12. Bouvier, J. et al. Descending command neurons in the brainstem that halt locomotion. *Cell* **163**, 1191–1203 (2015).
13. Juvin, L. et al. A specific population of reticulospinal neurons controls the termination of locomotion. *Cell Rep.* **15**, 2377–2386 (2016).
14. Grillner, S. et al. Intrinsic function of a neuronal network—a vertebrate central pattern generator. *Brain Res. Brain Res. Rev.* **26**, 184–197 (1998).
15. Brocard, F. et al. The transformation of a unilateral locomotor command into a symmetrical bilateral activation in the brainstem. *J. Neurosci.* **30**, 523–533 (2010).
16. Shik, M. L., Severin, F. V. & Orlovskii, G. N. Control of walking and running by means of electric stimulation of the midbrain. *Biofizika* **11**, 659–666 (1966).
17. Shefchyk, S. J., Jell, R. M. & Jordan, L. M. Reversible cooling of the brainstem reveals areas required for mesencephalic locomotor region evoked treadmill locomotion. *Exp. Brain Res.* **56**, 257–262 (1984).
18. Garcia-Rill, E. & Skinner, R. D. The mesencephalic locomotor region. I. Activation of a medullary projection site. *Brain Res.* **411**, 1–12 (1987).
19. Garcia-Rill, E. & Skinner, R. D. The mesencephalic locomotor region. II. Projections to reticulospinal neurons. *Brain Res.* **411**, 13–20 (1987).
20. Bachmann, L. C. et al. Deep brain stimulation of the midbrain locomotor region improves paraparetic hindlimb function after spinal cord injury in rats. *Sci. Transl. Med.* **5**, 208ra146 (2013).
21. Ferreira-Pinto, M. J., Ruder, L., Capelli, P. & Arber, S. Connecting circuits for supraspinal control of locomotion. *Neuron* **100**, 361–374 (2018).
22. Steinmetz, N. A., Zatka-Haas, P., Carandini, M. & Harris, K. D. Distributed coding of choice, action and engagement across the mouse brain. *Nature* **576**, 266–273 (2019).
23. Hägglund, M. et al. Optogenetic dissection reveals multiple rhythmicogenic modules underlying locomotion. *Proc. Natl Acad. Sci. USA* **110**, 11589–11594 (2013).
24. Kjaerulff, O. & Kiehn, O. Distribution of networks generating and coordinating locomotor activity in the neonatal rat spinal cord in vitro: a lesion study. *J. Neurosci.* **16**, 5777–5794 (1996).
25. Bracci, E., Ballerini, L. & Nistri, A. Localization of rhythmicogenic networks responsible for spontaneous bursts induced by strychnine and bicuculline in the rat isolated spinal cord. *J. Neurosci.* **16**, 7063–7076 (1996).
26. Bonnot, A., Whelan, P. J., Mentis, G. Z. & O'Donovan, M. J. Locomotor-like activity generated by the neonatal mouse spinal cord. *Brain Res. Brain Res. Rev.* **40**, 141–151 (2002).
27. Kremer, E. & Lev-Tov, A. Localization of the spinal network associated with generation of hindlimb locomotion in the neonatal rat and organization of its transverse coupling system. *J. Neurophysiol.* **77**, 1155–1170 (1997).
28. Muir, G. D. & Whishaw, I. Q. Complete locomotor recovery following corticospinal tract lesions: measurement of ground reaction forces during overground locomotion in rats. *Behav. Brain Res.* **103**, 45–53 (1999).
29. Jin, D. et al. Restoration of skilled locomotion by sprouting corticospinal axons induced by co-deletion of PTEN and SOCS3. *Nat. Commun.* **6**, 8074 (2015).
30. Deliagina, T. G., Popova, L. B. & Grant, G. The role of tonic vestibular input for postural control in rats. *Arch. Ital. Biol.* **135**, 239–261 (1997).
31. Armbruster, B. N., Li, X., Pausch, M. H., Herlitze, S. & Roth, B. L. Evolving the lock to fit the key to create a family of G protein-coupled receptors potently activated by an inert ligand. *Proc. Natl Acad. Sci. USA* **104**, 5163–5168 (2007).
32. Hägglund, M., Borgius, L., Dougherty, K. J. & Kiehn, O. Activation of groups of excitatory neurons in the mammalian spinal cord or hindbrain evokes locomotion. *Nat. Neurosci.* **13**, 246–252 (2010).
33. Kjaerulff, O. & Kiehn, O. Crossed rhythmic synaptic input to motoneurons during selective activation of the contralateral spinal locomotor network. *J. Neurosci.* **17**, 9433–9447 (1997).
34. Mathis, A. et al. DeepLabCut: markerless pose estimation of user-defined body parts with deep learning. *Nat. Neurosci.* **21**, 1281–1289 (2018).
35. Bellardita, C. & Kiehn, O. Phenotypic characterization of speed-associated gait changes in mice reveals modular organization of locomotor networks. *Curr. Biol.* **25**, 1426–1436 (2015).
36. Wall, N. R., Wickersham, I. R., Cetin, A., De La Parra, M. & Callaway, E. M. Monosynaptic circuit tracing in vivo through Cre-dependent targeting and complementation of modified rabies virus. *Proc. Natl Acad. Sci. USA* **107**, 21848–21853 (2010).
37. Liu, K. et al. Lhx6-positive GABA-releasing neurons of the zona incerta promote sleep. *Nature* **548**, 582–587 (2017).
38. Zingg, B. et al. AAV-mediated anterograde transsynaptic tagging: mapping corticocollicular input-defined neural pathways for defense behaviors. *Neuron* **93**, 33–47 (2017).
39. Shang, C. et al. A parvalbumin-positive excitatory visual pathway to trigger fear responses in mice. *Science* **348**, 1472–1477 (2015).
40. Felsen, G. & Mainen, Z. F. Neural substrates of sensory-guided locomotor decisions in the rat superior colliculus. *Neuron* **60**, 137–148 (2008).
41. Oliveira, A. F. & Yonehara, K. The mouse superior colliculus as a model system for investigating cell type-based mechanisms of visual motor transformation. *Front. Neural Circuits* **12**, 59 (2018).
42. Borgius, L., Restrepo, C. E., Leao, R. N., Saleh, N. & Kiehn, O. A transgenic mouse line for molecular genetic analysis of excitatory glutamatergic neurons. *Mol. Cell. Neurosci.* **45**, 245–257 (2010).
43. Fagerstedt, P., Orlovsky, G. N., Deliagina, T. G., Grillner, S. & Ullén, F. Lateral turns in the lamprey. ii. Activity of reticulospinal neurons during the generation of fictive turns. *J. Neurophysiol.* **86**, 2257–2265 (2001).
44. Huang, K. H., Ahrens, M. B., Dunn, T. W. & Engert, F. Spinal projection neurons control turning behaviors in zebrafish. *Curr. Biol.* **23**, 1566–1573 (2013).
45. Kozlov, A. K., Kardamakis, A. A., Hellgren Kotaleski, J. & Grillner, S. Gating of steering signals through phasic modulation of reticulospinal neurons during locomotion. *Proc. Natl Acad. Sci. USA* **111**, 3591–3596 (2014).
46. Thiele, T. R., Donovan, J. C. & Baier, H. Descending control of swim posture by a midbrain nucleus in zebrafish. *Neuron* **83**, 679–691 (2014).
47. Gruntman, E., Benjamini, Y. & Golani, I. Coordination of steering in a free-trotting quadruped. *J. Comp. Physiol. A Neuroethol. Sens. Neural Behav. Physiol.* **193**, 331–345 (2007).
48. Kimura, Y. alx, a zebrafish homolog of Chx10, marks ipsilateral descending excitatory interneurons that participate in the regulation of spinal locomotor circuits. *J. Neurosci.* **26**, 5684–5697 (2006).
49. Bagnall, M. W. et al. Glycinergic projection neurons of the cerebellum. *J. Neurosci.* **29**, 10104–10110 (2009).
50. Muzzu, T., Mitolo, S., Gava, G. P. & Schultz, S. R. Encoding of locomotion kinematics in the mouse cerebellum. *PLoS ONE* **13**, e0203900 (2018).

Publisher's note Springer Nature remains neutral with regard to jurisdictional claims in published maps and institutional affiliations.

© The Author(s), under exclusive licence to Springer Nature America, Inc. 2020

Methods

Mice. All animal experiments and procedures were approved by

Dyreforsøgstilsynet in Denmark and the local ethics committee at the University of Copenhagen (Nature Research Reporting Summary). The *Chx10^{Cre}* mouse is the same as that used previously^{12,51}. The *Vglut2^{Cre}* mouse is described in ref. ⁴². *R26R^{ChR2-EYFP}* mice were obtained from Jackson Laboratories (Jackson Stock, catalog no. 012569). For in vitro experiments, we used newborn mice from *Chx10^{Cre}* and *R26R^{ChR2-EYFP}* crosses (Nature Research Reporting Summary). For in vivo experiments, we used hemizygous *Chx10^{Cre}*, *Vglut2^{Cre}* or WT mice (C57BL/6J, Jackson Stock, catalog no. 000664) aged >8 weeks. Experiments were performed with similar numbers of male and female mice.

Stereotaxic injections. Viral injections in adult mice were performed using a stereotactic injection system (Neurostar). Mice were anesthetized with 4% isofluorane, and maintained under anesthesia with 2% isofluorane for the duration of the surgery. Anesthetic depth was verified using a toe-pinch test. Virus was mixed with Fast Green dye for visualization, and injected using a glass micropipette at a rate of 100 nl min⁻¹. The glass micropipette was held in place for 5 min after injection to prevent backflow.

For unilateral anterograde tracing from the Gi to the spinal cord, we injected 250 nl AAV1-*phSyn1(S)-FLEX-tdTomato-T2A-SypEGFP-WPRE* (5.56×10^{11} ml⁻¹, Viral Vector Core, Salk Institute for Biological Sciences; Addgene, catalog no. 51509)⁵² into *Chx10^{Cre}* mice aged at least 8 weeks. Mice were perfused 6 weeks after injection. All injections into the Gi were made at -6.0 mm anteroposterior (AP), ± 0.8 mm mediolateral (ML) and -5.5 mm dorsoventral (DV) relative to bregma.

For experiments using excitatory hM3Dq-DREADDs, *Chx10^{Cre}* mice aged at least 8 weeks were injected in either the left or the right Gi with 500 nl AAV5-hSy n1-DIO-hM3D(Gq)-mCherry-WPRE (6×10^{12} ml⁻¹, Viral Vector Facility, University of Zurich, v.89) or 500 nl AAV5-hSyn1-DIO-mCherry control virus (1.3×10^{13} ml⁻¹, Viral Vector Facility, University of Zurich, v.116). Experiments were performed 3–6 weeks after injection. For in vivo optogenetics experiments, *Chx10^{Cre}* mice were injected with 500 nl AAVdj-Ef1a-DIO-hChR2(E123T/T159C)-P2A-mCherry-WPRE in the left or right Gi. Optical fibers were implanted 3 weeks later at -6 mm AP, ± 0.5 mm MLA and -4.8 mm DV relative to bregma, and photostimulation experiments were performed the next day. For experiments using tetanus toxin virus, we injected either 300 or 500 nl AAV1-FLEX-TeLC-EGFP to inhibit *Chx10* Gi neurons^{12,53}, or 500 nl AAV5-FLEX-EGFP as a control. Tetanus toxin behavioral experiments were performed within 9 d of viral injection. For inhibitory DREADDs, *Chx10^{Cre}* mice were injected with 350 nl AAV5-FLEX-hM4Di-mCherry in the left or right Gi (7.4×10^{12} ml⁻¹, Viral Vector Facility, University of Zurich, v.84). Experiments were performed 3–6 weeks after injection.

For rabies transsynaptic labeling, the left Gi was injected with 200 nl of a 1:1 mixture by volume of AAV1-syn-FLEX-splitTVA-EGFP-tTA (Addgene, catalog no. 100798) (diluted 200-fold to 8.5×10^{10} ml⁻¹) and AAV1-TREtight-mTagBFP2-B19G (Addgene, catalog no. 100799) (diluted 20-fold to 1.6×10^{12} ml⁻¹)³⁷. After 7 d, we injected 500 nl RVΔG-4mCherry(EnvA) (1.70×10^{10} infectious units ml⁻¹) into the same location. Mice were perfused 7 d after the second injection. The synthesis of pAAV-syn-FLEX-splitTVA-EGFP-tTA, pAAV-TREtight-mTagBFP2-B19G and RVΔG-4mCherry(EnvA) has been described previously^{37,54}.

For targeting the SC–Gi projection, injection of AAV-DIO-hM3Dq-mCherry or AAV5-dFRT-hM3Dq-mCherry (3.5×10^{12} ml⁻¹, Viral Vector Facility, University of Zurich, v.189-5) was followed 1 week later by injection of AAV_{retro}-EGFP-Cre (1.3×10^{13} ml⁻¹, Addgene, 105540-AAVrg), AAV_{retro}-FLEX-EGFP-2A-FlpO (6.8×10^{12} ml⁻¹, Viral Vector Facility, University of Zurich, v.171-retro), AAV1-EGFP-Cre (1×10^{13} ml⁻¹, Addgene, 105540-AAV1) or AAV1-FLEX-EGFP-2A-FlpO (7.3×10^{12} ml⁻¹, Viral Vector Facility, University of Zurich, v.171-1). Behavioral experiments were performed 1–2 weeks after the second viral injection. For retrograde targeting of SC–Gi projection neurons in WT mice, 80 nl AAV-DIO-hM3Dq-mCherry was injected into the contralateral SC and 150 nl AAV_{retro}-EGFP-Cre into the ipsilateral Gi. For anterograde targeting of SC–Gi postsynaptic neurons in WT mice, 40 nl AAV1-EGFP-Cre was injected into the contralateral SC and 150 nl AAV-DIO-hM3Dq-mCherry into the ipsilateral Gi. For retrograde targeting of SC–Gi projection neurons in *Vglut2^{Cre}* mice, 80 nl AAV-dFRT-hM3Dq-mCherry was injected into the contralateral SC and 150 nl AAV_{retro}-FLEX-EGFP-2A-FlpO into the ipsilateral Gi. For anterograde targeting of SC–Gi *Chx10* postsynaptic neurons in *Chx10^{Cre}* mice, 80 nl AAV1-FLEX-EGFP-2A-FlpO was injected into the contralateral SC and 500 nl AAV-dFRT-hM3Dq-mCherry into the ipsilateral Gi. SC coordinates used for these experiments were based on localization of RVΔG-4mCherry(EnvA)-labeled cells⁵⁵: SC: -3.5 mm AP, ± 1.12 mm ML and -2.15 mm DV relative to bregma.

In vivo optogenetics. Optical fibers (200-μm core, numerical aperture (NA) 0.22; Thorlabs) were implanted 3 weeks after ChR2 viral injection (see information under “Stereotaxic injections”). Photostimulation experiments were carried out the day after implantation. Fibers were held in a 1.25-mm ferrule, and coupled to a 473-nm laser (Optoduet, Ikecool Corporation) via a ceramic mating sleeve. Photostimuli were manually triggered via a transistor-transistor logic (TTL)-pulse given by Ethovision to a Master-8 pulse generator. Laser photostimulation was

carried out at 40 Hz (1-s train of 10-ms pulses), where the laser power was adjusted between 5 and 20 mW to initiate a strong turning response in each animal.

In vivo EMG. *Chx10^{Cre}* mice were injected with 500 nl AAVdj-Ef1a-DIO-hChR2(E123T/T159C)-P2A-mCherry-WPRE in the left or right Gi and implanted with an optical fiber (200-μm core, NA 0.22; Thorlabs). Mice were anesthetized intraperitoneally with a cocktail of ketamine (100 mg kg⁻¹) and xylazine (10 mg kg⁻¹). Body temperature was maintained on a heating pad throughout the experiment. Muscles in the neck (splenius capitis), abdomen (abdominal oblique) and hindlimbs (tibialis anterior and soleus) were exposed bilaterally. Two stainless steel wires—Teflon coated except for the tip (A-M Systems, catalog no. 790700)—were inserted into each muscle for bilateral bipolar EMG recordings. EMG signals were amplified 5,000–10,000 times, band-pass filtered from 100 Hz to 1 kHz, sampled at a frequency of 5 kHz (AxoScope, Molecular Devices) and digitally converted (Digidata 1440A, Molecular Devices). Muscle activity was assessed in response to optogenetic stimulation of *Chx10* Gi neurons using a 473-nm laser triggered via a TTL-pulse given by a Master-8 pulse generator. Laser power, graded between 5 and 20 mW, and light stimuli were applied as either a single 20-ms pulse or a five-pulse train at 50 Hz and 10 ms pulse duration. Data were analyzed using Spike2 (Cambridge Electronic Design). When the single-pulse stimulation had an effect, 50 Hz stimulation was performed at the same laser power. Multiple recordings were performed in each mouse and mice were euthanized at the termination of the experiments.

In vitro recording and optogenetics. Locomotor-like activity was recorded from in vitro, brainstem–spinal cord preparations isolated from P0-4 *Chx10^{Cre};R26R^{ChR2-EYFP}* mice. Neonatal mice were anesthetized and decapitated at the level of the midbrain. Mice were then eviscerated, and the base of the skull and vertebral bodies were quickly removed ventrally from the level of the rostral pons caudally to the sacral spinal cord under ice-cold oxygenated dissection buffer (95% O₂/5% CO₂, 4°C) composed of 111 mM NaCl, 3 mM KCl, 26 mM NaHCO₃, 1.1 mM KH₂PO₄, 0.25 mM CaCl₂, 3.7 mM MgCl₂, and 11 mM D-glucose. The ventral roots were cut at their point of exit from the vertebral canal. The caudal neuroaxis was then isolated from the vertebral canal, and a coronal section was performed at the level of the facial motor nucleus (VII), rostral to the anteroinferior cerebellar artery. The rostral aspect of the preparation was maintained in an upward position to allow access for optical stimulation¹². Alternatively, the brainstem was split along the midline from the most rostral part to C1. The optical stimulation was then performed unilaterally from the cut surface.

A two-compartment system was used for pharmacologic separation of the brainstem and lumbar spinal cord. The preparation was pinned to a Sylgard stage, and Vaseline was applied to the upper thoracic spinal cord at ~Th1. A peristaltic pump was used to separately perfuse the rostral (brainstem) and caudal (lumbar spinal cord) compartments with oxygenated recording buffer (95% O₂/5% CO₂, 22–24°C), composed of 111 mM NaCl, 3 mM KCl, 26 mM NaHCO₃, 1.1 mM KH₂PO₄, 2.5 mM CaCl₂, 1.25 mM MgCl₂, and 11 mM D-glucose. Kynurenic acid (4 mM; Sigma) was applied to the brainstem compartment to block all glutamatergic transmission in the brainstem, thereby isolating the contribution of *Chx10* reticulospinal neurons to spinal circuits¹². A cocktail of NMDA (6–8 μM; Sigma) and serotonin (6–15 μM; Sigma), sometimes with dopamine (50–100 μM; Sigma), was applied to the lumbar spinal cord compartment to initiate locomotor-like activity. Fast Green dye was maintained within the rostral compartment to verify an intact diffusion barrier, that is, drugs from the rostral compartment did not mix with the caudal compartment and vice versa.

Bipolar suction electrodes were attached to the left and right L2 and L5 ventral roots, and/or to the left and right thoracic ventral roots. The signals were amplified 5,000–10,000 times, band-pass filtered from 100 Hz to 1 kHz, and sampled at a frequency of 1 kHz with AxoScope (Molecular Devices). Optogenetic stimulation of ChR2-expressing neurons was performed using a 473-nm laser system (UGA-40; Rapp Optoelectronic), which delivered blue light at an intensity of 30 mW mm⁻² (ref. ⁵⁶). Blue light was directed at the preparation using an optical fiber (200-μm core, NA 0.22, Thorlabs). Photoillumination was carried out continuously for 2–5 s. The frequency of locomotor-like activity and burst amplitude (Fig. 4f,g) was analyzed from rectified, integrated (bin = 0.25 s) traces (using Spike2, Cambridge Electronic Design) from those bursts occurring 10 s before, 5 s during and 10 s after light stimulation. Five to eleven trials were quantified for each animal. To generate intensity plots for individual trials, rectified and integrated traces were exported, and then normalized in amplitude from 0 (representing the minimum time-series value in a trial) to 1 (maximum value).

To block inhibition in the spinal cord, PTX (5–10 μM; Sigma) was added to the caudal pool in the presence of locomotor-inducing drugs.

Limb dynamics. DeepLabCut^{34,57} was used for markerless extraction of paw position in an open field. DeepLabCut v2.0 was installed on a PC equipped with a GeForce RTX 2080 Ti graphics card. We captured videos of mice moving from below (50 frames per second (f.p.s.)). Body center position was tracked using Ethovision XT, and video segments were extracted for locomotor bouts directed through the center of the arena, which were >5 cm s⁻¹ and >15 cm long. The four paws, the tip of the nose and the base of the tail were tracked using DeepLabCut v2.0; 700 frames

were selected for labeling from videos representing different behavioral sessions. The network was trained for 600,000 iterations until the loss reached a plateau. Segments of recording with a likelihood <0.9 for any marker were excluded.

Subsequent analyses of limb kinematics were made using custom scripts in Python v.3.7. The body angle was defined as tail base–nose angle relative to the x axis. The velocity of each paw was used to define steps. Steps were first detected as consecutive points where paw velocity passed above/below 25 cm s⁻¹. The detection was further refined by defining the beginning of the swing phase as the point where paw velocity passed above 9 cm s⁻¹, and the end of the swing phase (that is, the beginning of the stance phase) as the point where paw velocity passed back below 9 cm s⁻¹. During alternating gaits, including fast walk and trot, mice move forward through the environment using diagonals—that is one forelimb and the contralateral hindlimb. Diagonal steps were defined as those occurring the closest in time for diagonal limbs. For each step, stride length was calculated as the length of the segment between the beginning and the end of the swing phase. We compared differences in stride length between the left and right sides with body angle at the beginning and end of a diagonal step. Pearson's correlation coefficient was used to estimate how stride length correlated with body angle.

Tissue immunochemistry and imaging. Mice were euthanized by anesthetic overdose with pentobarbital (250 mg kg⁻¹), and perfused transcardially with 4°C saline followed by 4% paraformaldehyde. Brain and spinal cord tissue was dissected free, and then postfixed in 4% paraformaldehyde for 3 h at 4°C. Tissue was cryoprotected by incubation in 30% sucrose in phosphate-buffered saline (PBS) overnight. Tissue was then embedded in Neg-50 medium (Thermo Fisher Scientific) for cryostat sectioning. Coronal or sagittal sections were obtained on a Leica or a CryoStar NX70 cryostat and mounted on Superfrost Plus slides (Thermo Fisher Scientific). Brainstem coronal sections were cut at 30 µm thickness, whereas spinal cord coronal sections were cut at 20 µm. Sagittal sections were cut at 30 µm.

Sections were rehydrated for 5 min in PBS + 0.5% Triton-X100 (PBS-T; Sigma-Aldrich), and then blocked for 2 h in 10% normal donkey serum in PBS-T (Jackson ImmunoResearch). Sections were incubated overnight with primary antibodies diluted in blocking solution. We used the following primary antibodies: chicken anti-green fluorescent protein (GFP) (1:1,000, Abcam, ab13970) and rabbit anti-DsRed/tdTomato/mCherry (1:1,000, Clontech, catalog no. 632496). The specificity of primary antibodies was validated in previous publications as indicated in the Antibody Registry (Nature Research Reporting Summary). Slides were washed four times in PBS-T, and then incubated with appropriate donkey secondary antibodies diluted in blocking solution (1:500, Thermo Fisher Scientific). Slides were washed four times in PBS-T, counterstained with Hoechst 33342 (1:2,000) or NeuroTrace 435 (1:400, Thermo Fisher Scientific) and mounted with coverslips using mowiol 4–88 medium. Sections were imaged using either a Zeiss widefield epifluorescence microscope or a Zeiss LSM 780 confocal microscope.

Drugs. CNO (Tocris, catalog no. 4936) was dissolved in saline immediately before behavioral experiments. It was administered intraperitoneally at a dose of 0.5 mg kg⁻¹ (*Chx10*^{Cre}>FLEX-hM3Dq; Fig. 2, and Extended Data Figs. 2, 3 and 6) or 1 mg kg⁻¹ (*Chx10*^{Cre}>FLEX-hM4Di, Fig. 3; SC or Gi>FLEX-hM3Dq or dFRT-hM3Dq, Fig. 7).

Cylinder test. Mice were placed in a 15-cm diameter cylinder for 10 min. Ethovision XT (Noldus) software was used to capture video (15 f.p.s.) and carry out tracking of head, center point and tail; 360° clockwise and counterclockwise revolutions were quantified (tail point to center point, 50° threshold).

Open field. Mice were acclimated to the behavioral suite before testing in an open-field arena. Open-field analysis was carried out in a 50 × 50 cm² arena illuminated with an infrared lamp. Ethovision XT (Noldus) software was used to capture video (15–25 f.p.s.) and carry out tracking analysis. Mice were tracked using head, center and tail points, enabling quantification of rotations as a function of time. Movement parameters taken in the open field included 360° revolutions (tail point to center point, 50° threshold), velocity of locomotor bouts (bouts of locomotion were defined as periods during which the animal moved at a velocity >2 cm s⁻¹), total movement (m), ambulation (time moving at a velocity >2 cm s⁻¹) and stops per minute (instances where velocity fell <2 cm s⁻¹). Tracking was carried out for 60 min. Mice were allowed to acclimate to the arena for 30 min, followed by a 30-min probe. Movement parameters are reported for minutes 30–60.

Ipsilateral–contralateral spiral maze. Spiral-shaped mazes were used to test clockwise/counterclockwise movement preference. For this purpose, mazes were fabricated that could be explored from the center point to the periphery only by moving in a clockwise or counterclockwise direction (Fig. 6a,c). These mazes exhibit an increasing radius as mice move from the center point to the periphery. For each mouse, a 10-min trial was conducted in either the left- or the right-turned maze. One affected mouse exhibited a turning radius that was smaller than the center of the maze (Fig. 6a,c). This affected mouse was excluded from analysis because it could not complete either the ipsilateral or the contralateral maze. Body tracking was carried out with Ethovision XT using center-point detection.

Analysis. For quantification of viral transduction in the Gi, the numbers of neurons ipsilateral and contralateral to the injection site were counted in every tenth section. These counts were used to estimate the percentage of viral transduction contained to the ipsilateral side (Fig. 1). Similar analysis was performed to estimate the percentage of labeled neurons in the ipsilateral versus the contralateral SC (Fig. 7).

For analysis of synGFP⁺ punctae in tdTom-2A-synGFP-traced projections, high-resolution images of GFP-stained coronal spinal cord sections were obtained with a confocal microscope. Three images from each spinal level (that is, cervical, thoracic and lumbar) were quantified from three mice. Analysis of synGFP punctae was restricted to the gray matter, with the assumption that synGFP punctae in the white matter reflected transport of synGFP protein rather than bona fide synapses. SynGFP punctae were isolated from the images using thresholding, and the position of each punctum was extracted using the particle analysis feature in ImageJ (<https://imagej.nih.gov/ij>). The position of the central canal was defined using the Nissl counterstain, and the synGFP punctae position was normalized between sections and mice using this point as a reference. From this dataset, the percentage of synapses ipsilateral and contralateral to the injection site was estimated (Fig. 1). Synaptic density plots were constructed in R, where gradation represents the range from zero to maximum density at each spinal level (Fig. 1g). Synaptic density plots represent the average of six mice. Coordinates and abbreviations are based on Paxinos and Franklin's reference atlas⁵⁵, and corresponding plates are from the Allen Mouse Brain Atlas⁵⁸.

Statistics. No statistical methods were used to predetermine sample sizes; our sample sizes are similar to those reported in previous publications (Nature Research Reporting Summary)^{5,59,60}. Mice were randomly allocated to different groups for the in vivo experiments using a block design. Data collection and analysis were not performed blind to the conditions of the experiments, but the analysis was automated so that the experimenter had no influence on the outcome. Mice that did not react to experimental perturbations (CNO or light) were excluded from analysis only if it was confirmed that the viral infection was not present or off target. This exclusion was done after the experiments because it required analysis of tissue from the animal. A paired, two-tailed Student's *t*-test was performed for pairwise comparisons. For multiple comparisons, a one-, two- or three-way analysis of variance (ANOVA) (with repeated measures where appropriate) was performed to determine whether significant differences existed between conditions, followed by multiple comparison testing using the Tukey-Kramer honestly significantly different test. Data distribution was assumed to be normal but this was not formally tested. An *F*-test was used to determine significance in regression analyses. Data are plotted with box-and-whisker plots, which give the median, the 25th and 75th percentiles, and the range. Time-series data tracking movement preference in the open field and individual *n* in linear regression are given as mean ± s.e.m. Individual data points are plotted for each comparison, and information on statistical analyses, *P* value statistics and *n* values is listed in the figure legends, as well as in Supplementary Table 1. The *n* values represent distinct biological replicates (mice), except for regression analyses in Extended Data Fig. 6, where *n* represents individual steps or locomotor bouts. The number of trials varied between mice. *P* < 0.05 was considered statistically significant, where **P* < 0.05, ***P* < 0.01 and ****P* < 0.001. Statistical analyses were carried out in Graphpad Prism v.8.3 or SAS JMP Pro v.15.

Reporting Summary. Further information on research design is available in the Nature Research Reporting Summary linked to this article.

Data availability

The data that support the findings of this study are available from the corresponding author upon reasonable request.

Code availability

The code used to analyze data and produce figure content is available from the corresponding author upon request.

References

- Azim, E., Jiang, J., Alstermark, B. & Jessell, T. M. Skilled reaching relies on a V2a propriospinal internal copy circuit. *Nature* **508**, 357–363 (2014).
- Oh, S. W. et al. A mesoscale connectome of the mouse brain. *Nature* **508**, 207–214 (2014).
- Murray, A. J. et al. Parvalbumin-positive CA1 interneurons are required for spatial working but not for reference memory. *Nat. Neurosci.* **14**, 297–299 (2011).
- Wickersham, I. R. & Sullivan, H. A. Rabies viral vectors for monosynaptic tracing and targeted transgene expression in neurons. *Cold Spring Harb. Protoc.* **4**, 375–385 (2015).
- Franklin, K. B. J. & Paxinos, G. *Paxinos and Franklin's the Mouse Brain in Stereotaxic Coordinates* (Academic Press, 2019).
- Bellardita, C. et al. Spatiotemporal correlation of spinal network dynamics underlying spasms in chronic spinalized mice. *eLife* **6**, e23011 (2017).

57. Nath, T. et al. Using DeepLabCut for 3D markerless pose estimation across species and behaviors. *Nat. Protoc.* **14**, 2152–2176 (2019).
58. Lein, E. S. et al. Genome-wide atlas of gene expression in the adult mouse brain. *Nature* **445**, 168–176 (2007).
59. Jennings, J. H. et al. Interacting neural ensembles in orbitofrontal cortex for social and feeding behaviour. *Nature* **565**, 645–649 (2019).
60. Evans, D. A. et al. A synaptic threshold mechanism for computing escape decisions. *Nature* **558**, 590–594 (2018).

Acknowledgements

We thank K. Sharma, L. Zagoraiou, S. Crone and T.M. Jessell for the *Chx10^{Ore}* mouse line. We acknowledge the Core Facility for Integrated Microscopy, Faculty of Health and Medical Sciences, University of Copenhagen. We thank I. Vesth-Hansen and D. Meinertz for technical assistance, and members of O.K.'s laboratory for discussion and comments on previous versions of this manuscript. This work was supported by an EMBO Long-Term Fellowship (to J.M.C., grant no. ALTF 421-2018), the European Research Council under the European Union's Horizon 2020 research and innovation program (to O.K., grant agreement no. REP-SCI-693038), the Novo Nordisk Laureate Program (to O.K., NNF15OC0014186), the Faculty of Health and Medical Sciences University of Copenhagen (to O.K. and A.M.) and the Swedish Resarch Council (to O.K.).

Author contributions

J.M.C. and O.K. conceptualized the study. J.M.C., R.L., A.M. and O.K. provided methodology. J.M.C., R.L., A.M. and P.W. carried out the investigations. I.R.W. provided resources. J.M.C. and O.K. wrote the original draft. J.M.C., R.L. and O.K. wrote, reviewed and edited the manuscript. O.K. supervised the study. J.M.C. and O.K. acquired funds.

Competing interests

The authors declare no competing interests.

Additional information

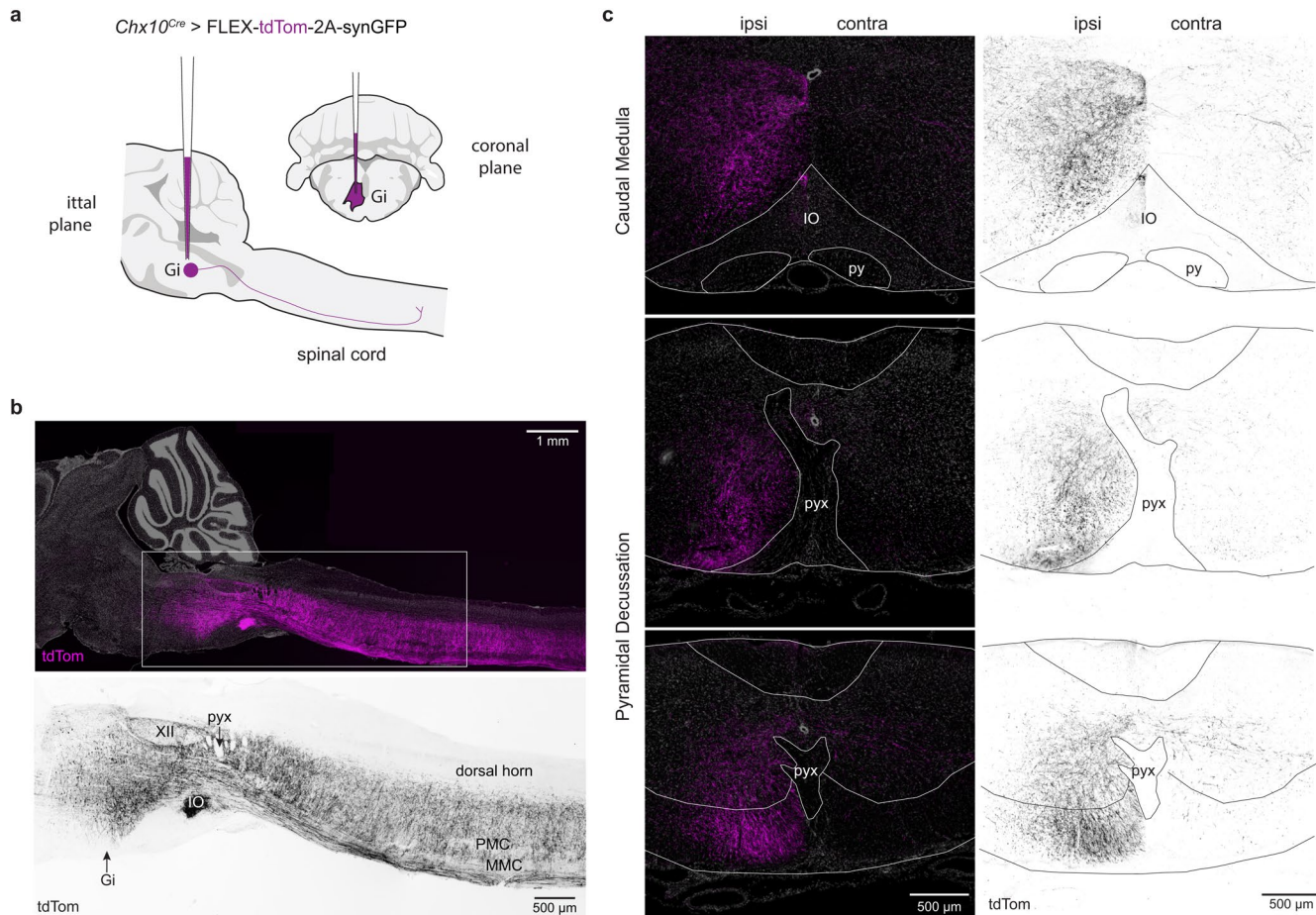
Extended data is available for this paper at <https://doi.org/10.1038/s41593-020-0633-7>.

Supplementary information is available for this paper at <https://doi.org/10.1038/s41593-020-0633-7>.

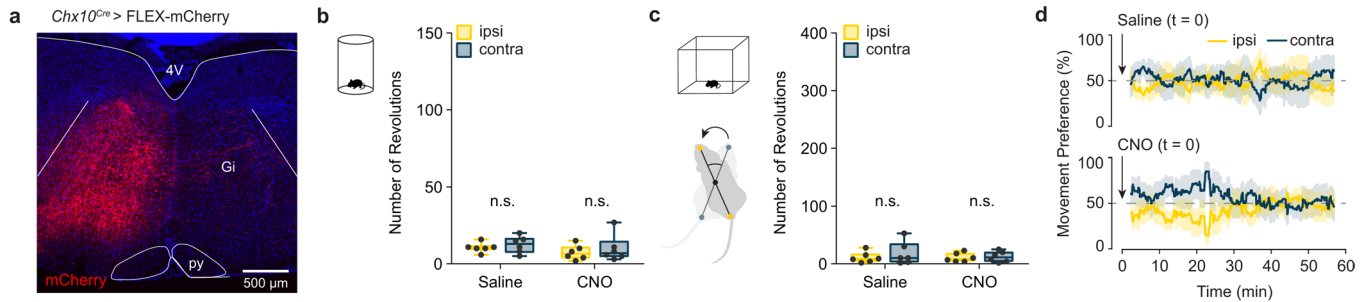
Correspondence and requests for materials should be addressed to O.K.

Peer review information *Nature Neuroscience* thanks Michael Fehlings and the other, anonymous, reviewer(s) for their contribution to the peer review of this work.

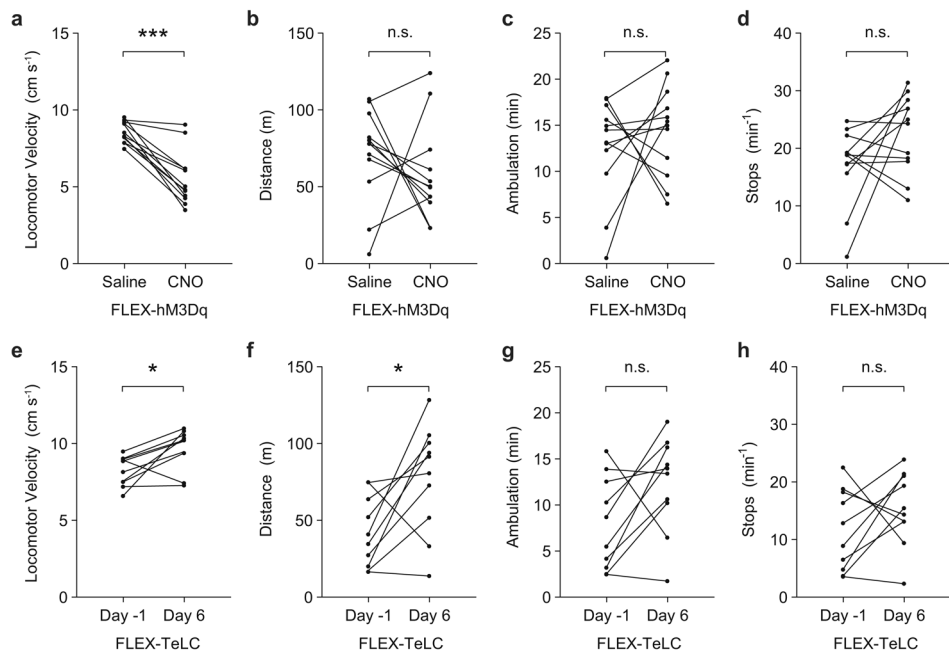
Reprints and permissions information is available at www.nature.com/reprints.



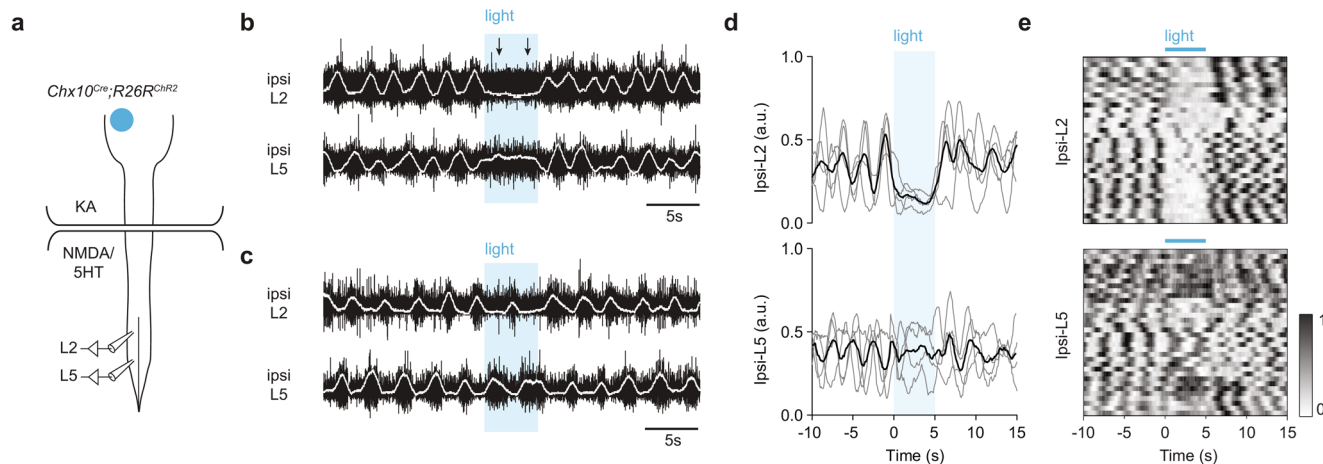
Extended Data Fig. 1 | *Chx10* Gi neurons form a prominent tract of ipsilaterally projecting axons. **a**, Unilateral labeling of *Chx10* neurons of the rostral gigantocellularis (Gi) using the Cre-dependent anterograde tracer AAV-FLEX-tdTom-2A-synGFP. **b**, *Top*, Sagittal section of tdTom⁺ projections ipsilateral to the injection site. tdTom⁺ axons formed a prominent tract that projected caudally to the spinal cord. *Bottom*, inset from *Top*. XII, hypoglossal motor nucleus; pyx, pyramidal decussation; IO, inferior olive; PMC, phrenic motor column; MMC, medial motor column. Images in **(b)** are representative of tracing experiments from $n = 3$ mice. **c**, Coalescence of *Chx10* reticulospinal axons dorsal to the inferior olive (*top*), and subsequent positioning in the ventrolateral funiculus at the level of the pyramidal decussation (*bottom*). Images in **(c)** are representative of tracing experiments from $n = 6$ mice.



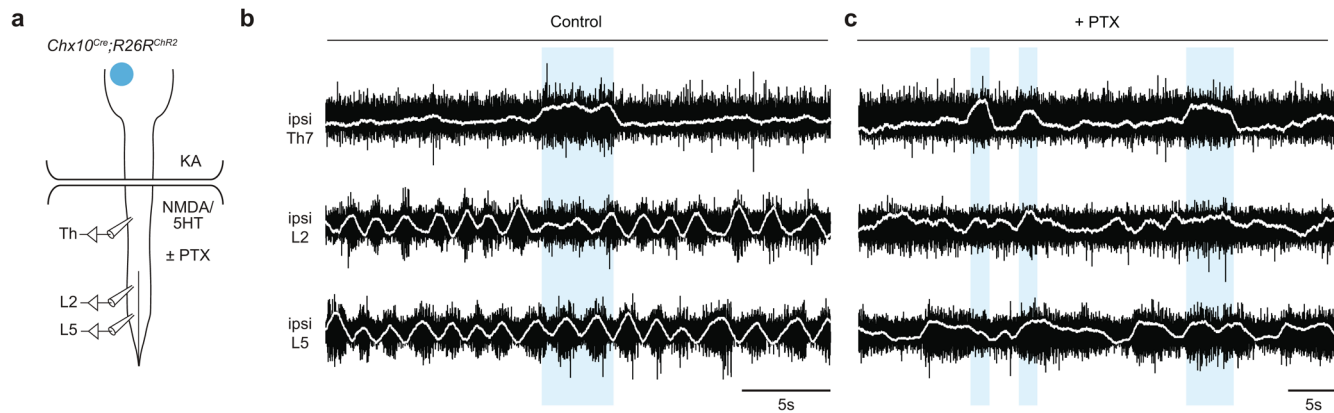
Extended Data Fig. 2 | CNO administration does not affect turning preference in control AAV-mCherry injected mice. **a**, Example of mCherry expression 3 weeks after a 500 nl unilateral injection of AAV-FLEX-mCherry in a *Chx10^{Cre}* mouse (representative image from $n = 6$ mice). mCherry expression is confined to the side ipsilateral to injection. **b**, Turning preference in a 10 minute cylinder assay is unaffected by administration of CNO. $P > 0.24$ (see Supplementary Table 1), two-way ANOVA with Tukey's multiple comparisons test, $n = 6$ mice from one experiment. **c**, Turning preference in an open field arena is unaffected by administration of CNO. $P > 0.42$, two-way ANOVA with Tukey's multiple comparisons test, $n = 6$ mice from one experiment. Box-and-whisker plots in **(c, d)** give the median, 25th and 75th percentiles, and range. **d**, Instantaneous quantification of ipsilateral and contralateral revolutions for mice in **(c)** after injection of either saline or CNO in AAV-FLEX-mCherry injected mice. Time-series data are plotted as mean \pm standard error mean.



Extended Data Fig. 3 | Analysis of open field locomotor performance in *Chx10*^{Cre} > FLEX-hM3Dq and *Chx10*^{Cre} > FLEX-TeLC mice. **a-d**, Open field locomotor performance in *Chx10*^{Cre} > FLEX-hM3Dq mice after administration of saline or CNO. CNO administration significantly decreased the velocity of locomotor bouts (**a**, ***P < 0.001, paired two-tailed t-test, n = 12 mice from three independent experiments), with no effect on the distance traveled (**b**, P = 0.40, paired two-tailed t-test, n = 12 mice), ambulation (**c**, P = 0.46, paired two-tailed t-test, n = 12 mice), or number of stops per minute (**d**, P = 0.11, paired two-tailed t-test, n = 12 mice). **e-h**, Open field locomotor performance in *Chx10*^{Cre} > FLEX-TeLC mice 1 day before injection versus 6 days after injection. TeLC expression significantly increased the velocity of locomotor bouts (**e**, *P = 0.015, paired two-tailed t-test, n = 10 mice from two independent experiments) and the distance traveled (**f**, *P = 0.022, paired two-tailed t-test, n = 10 mice from two independent experiments), with no effect on ambulation (**g**, P = 0.07, paired two-tailed t-test, n = 10 mice) or the number of stops per minute (**h**, P = 0.24, paired two-tailed t-test, n = 10 mice).

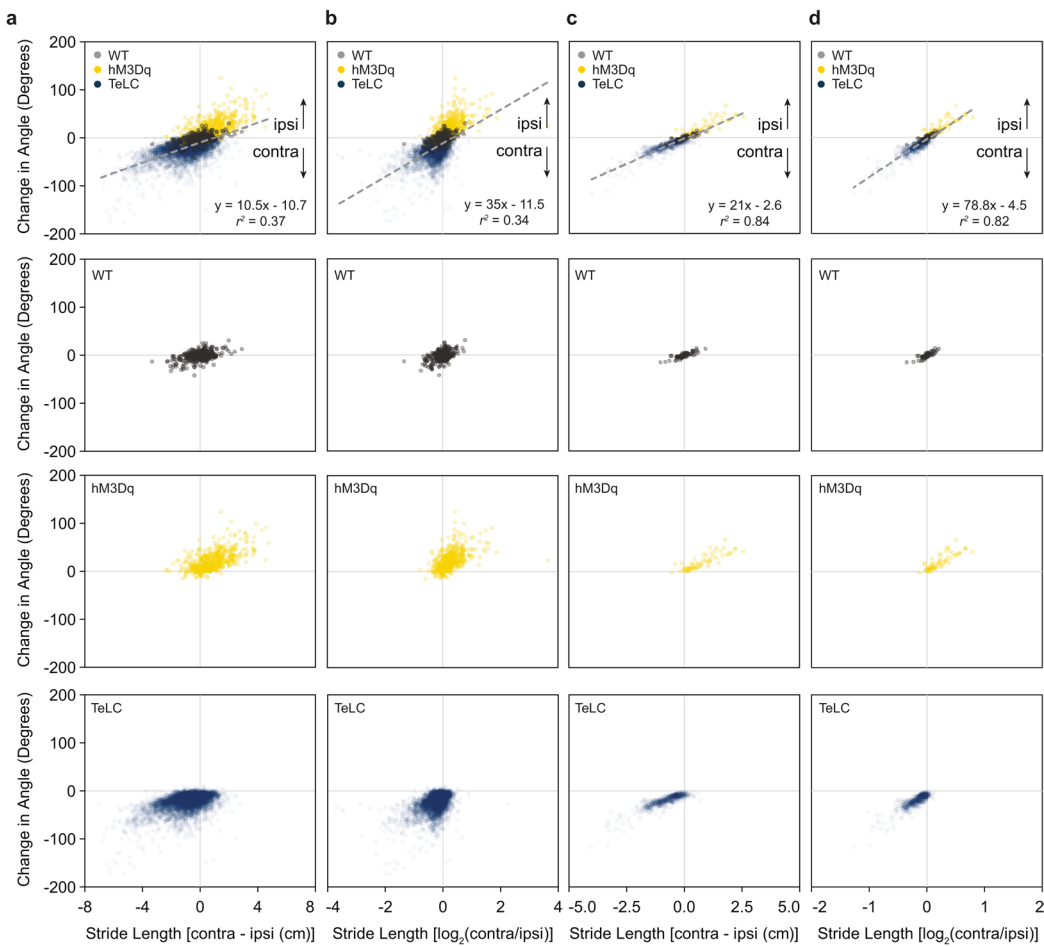


Extended Data Fig. 4 | Unilateral activation of *Chx10* Gi neurons causes inhibition of ipsilateral rhythmic flexor locomotor activity and prolongation of ipsilateral extensor locomotor activity. **a**, Schematic of split-bath brainstem-spinal cord preparation from *PO-4 Chx10^{Cre};R26R^{ChR2}* mice, as in Fig. 4. Recordings are taken from the ipsilateral L2 (flexor-related) and L5 (extensor-related) ventral roots. **b–c**, Unilateral photostimulation of *Chx10* Gi neurons reduces the frequency (**b**) and/or the amplitude (**c**) of locomotor-like flexor activity ipsilateral (ipsi L2) to the stimulation (compare with Fig. 4), with a simultaneous prolongation of extensor-related burst duration (ipsi L5). Traces in (**b,c**) are derived from two different mice and are representative of $n = 4$ independent preparations. **d**, Integrated traces normalized in amplitude from 0–1 and averaged across trials for each mouse ($n = 4$ mice, grey), with the grand average across mice represented in black. **e**, 33 trials from 4 mice represented as intensity plots from 0–1, which are integrated traces normalized from 0–1. 3 of the mice represented for ipsi-L2 are also represented in Fig. 4.



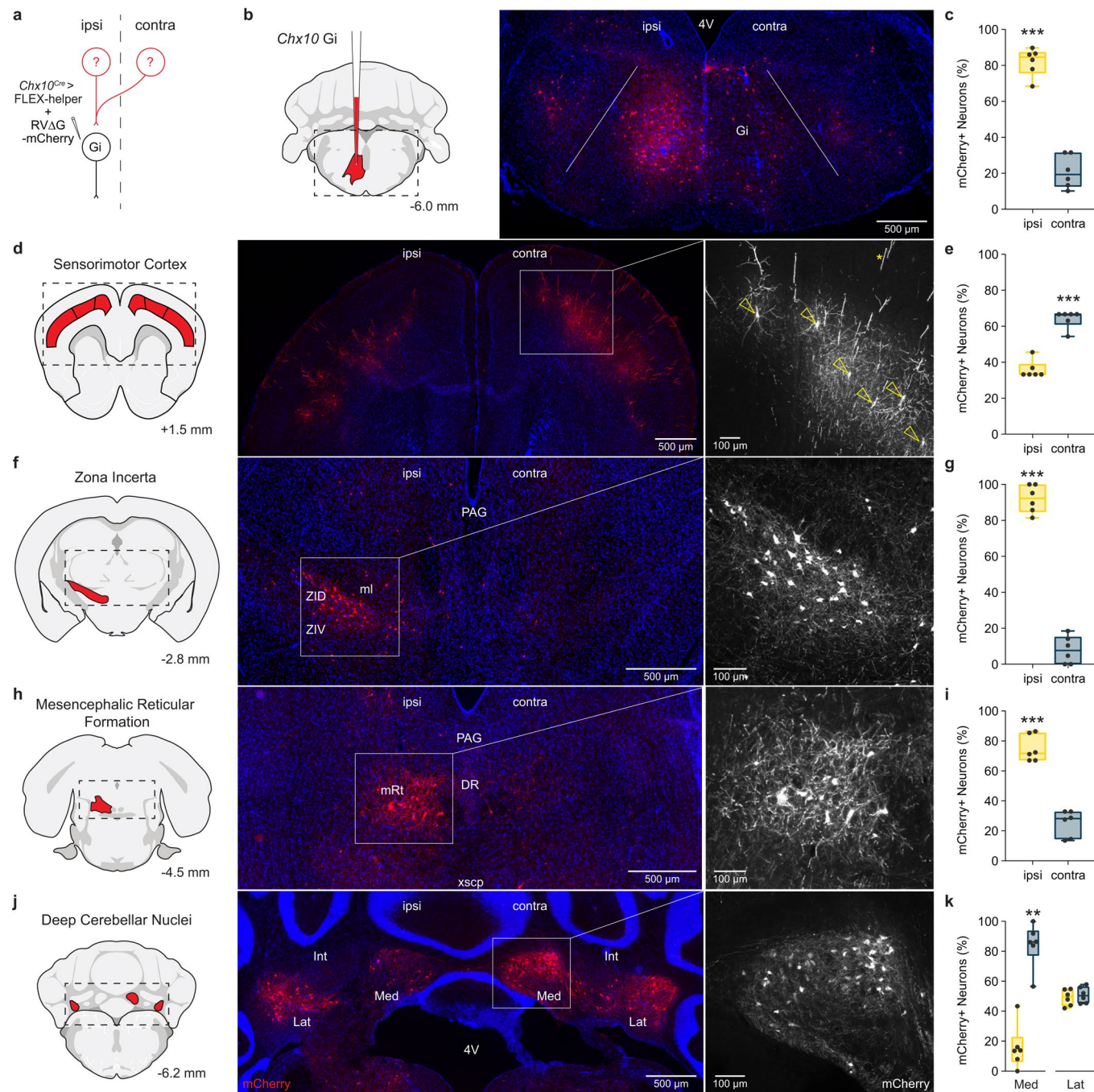
Extended Data Fig. 5 | Blocking inhibition in the spinal cord reveals an opposite effect of *Chx10* Gi stimulation on axial and locomotor networks.

a, Schematic of split-bath brainstem-spinal cord preparation from PO-P4 *Chx10^{Cre};R26R^{ChR2}* mice, as in Fig. 4. Recordings are taken from the ipsilateral thoracic (Th, axial), L2 (flexor-related), and L5 (extensor-related) ventral roots. Picrotoxin (PTX, 10 μ M) was added to the caudal pool to block inhibition in the spinal cord. **b**, Recordings from ipsilateral Th7, L2, and L5 ventral roots in presence of locomotor promoting drugs (NMDA/5HT) demonstrating that unilateral photostimulation of *Chx10* Gi neurons reduces the locomotor-like flexor activity ipsilateral (ipsi L2) to the stimulation, with a simultaneous prolongation of extensor-related burst durations (ipsi L5), and a tonic increase of thoracic activity lasting for the stimulus duration. ($n = 4$ independent preparations, 46 trials). **c**, In the presence of PTX, photostimulation of *Chx10* Gi neurons no longer affected rhythmic lumbar locomotor-like activity ($n = 5$ independent preparations, 69 trials), whereas activation of thoracic (axial) motor activity is still present.



Extended Data Fig. 6 | Stride length asymmetries versus heading position in wild-type, *Chx10^{Cre}* > FLEX-hM3Dq, and *Chx10^{Cre}* > FLEX-TeLC mice.

a, b, Analysis of individual steps relative to direction of movement in wild-type (WT), *Chx10^{Cre}* > FLEX-hM3Dq (hM3Dq), and *Chx10^{Cre}* > FLEX-TeLC (TeLC) mice. Stride length (cm) was measured on the ipsilateral and contralateral side together with the direction of movement. Stride length values are positive when the stride length is longer on the contralateral side. Positive changes in angle reflect an ipsilateral turn whereas negative values are contralateral. 6016 individual steps were analyzed from 6 wildtype (WT) (352 strides), 6 hM3Dq (477 strides), and 6 TeLC (5187 strides) mice. ***P < 0.001 for regression in (a) and (b), F-test, n = 6016 strides. **c-d,** Data for individual locomotor bouts (representing the average of all steps in a locomotor bout) from WT, hM3Dq, and TeLC mice. 708 locomotor bouts were analyzed from 6 WT (63 bouts), 6 hM3Dq (61 bouts), and 6 TeLC (584 bouts) mice. ***P < 0.001 for regression in (c) and (d), F-test, n = 708 locomotor bouts. Full information on regression analyses for WT, hM3Dq, TeLC, and pooled data can be found in Supplementary Table 1. Goodness of fit is given as the coefficient of determination (r^2 ; the square of Pearson's r).



Extended Data Fig. 7 | Monosynaptic rabies tracing identifies Chx10 Gi presynaptic inputs. **a**, A rabies transsynaptic tracing approach was used to identify presynaptic inputs to Chx10 Gi neurons (see also, Fig. 7 and Supplementary Table 2). **b**, Injection site in rostral Gi. Initial site of infection is visualized as a large population of mCherry+ neurons, accompanied by dense mCherry+ processes. Starter neurons of the ipsilateral Gi do not exhibit a strong input from neurons of the contralateral Gi. **c**, Quantification of mCherry-labeled neurons in the ipsilateral and contralateral Gi. ***P = 0.0002, paired two-tailed t-test, n = 6 mice from one experiment. **d**, Bilateral input to Chx10 Gi neurons from neurons of primary motor and somatosensory cortex. Open yellow triangles point to soma from pyramidal neurons. Yellow asterisk indicates an apical dendrite. **e**, Quantification of mCherry-labeled neurons in the ipsilateral and contralateral cortex. ***P = 0.001, paired two-tailed t-test, n = 6 mice from one experiment. **f**, Input to Chx10 Gi neurons from neurons of the ipsilateral zona incerta. Presynaptic neurons were observed primarily in the dorsal (ZID) and caudal aspects of the zona incerta. **g**, Quantification of mCherry-labeled neurons in the ipsilateral and contralateral zona incerta. ***P < 0.001, paired two-tailed t-test, n = 6 mice from one experiment. **h**, Unilateral input to Chx10 Gi neurons from the ipsilateral mesencephalic reticular formation. **i**, Quantification of mCherry-labeled neurons in the ipsilateral and contralateral mesencephalic reticular formation. ***P = 0.001, paired two-tailed t-test, n = 6 mice from one experiment. **j**, Medial (Med) and lateral (Lat) deep cerebellar nuclei exhibited unilateral or bilateral, respectively, input to Chx10 Gi neurons. **k**, Quantification of mCherry-labeled neurons in the deep cerebellar nuclei. Med, **P = 0.0024, paired two-tailed t-test, n = 6 mice from one experiment; Lat, P = 0.69, paired two-tailed t-test, n = 6 mice from one experiment. Box-and-whisker plots in **c, e, g, i, k** give the median, 25th and 75th percentiles, and range.